Uncovering the electrical synapse proteome in retinal neurons via *in vivo* proximity labeling

Stephan Tetenborg[1,8], Eyad Shihabeddin[1,9], Elizebeth Olive Akansha Manoj Kumar[1,9], Crystal L. Sigulinsky[2,9], Karin Dedek[3,4], Ya-Ping Lin[1], Fabio A. Echeverry[5], Hannah Hoff[5], Alberto E. Pereda[5], Bryan W. Jones[2], Christophe P. Ribelayga[1], Klaus Ebnet[6], Ken Matsuura[7] & John O'Brien[1,8]

[1]College of Optometry, University of Houston, Houston, TX, United states.
[2]Moran Eye Center/Ophthalmology, University of Utah, Salt Lake City, Utah, United states.
[3]Animal Navigation/ Neurosensorics, Institute for Biology and Environmental Sciences, University of Oldenburg, Oldenburg, Germany.
[4]Research Center Neurosensory Science, University of Oldenburg, Oldenburg, Germany.
[5]Dominick P. Purpura Department of Neuroscience, Albert Einstein College of Medicine, Bronx, New York, United States.
[6]Institute-Associated Research Group: Cell Adhesion and Cell Polarity, Institute of Medical Biochemistry, ZMBE, University of Münster, Münster, Germany.
[7]Cell Signal Unit, Okinawa Institute of Science and Technology, Onna-son 904-0495, Japan.
[8]To whom correspondence should be addressed
[9]Contributed equally

Correspondence: stetenbo@Central.UH.EDU (S.T.) and jobrien3@Central.UH.EDU (J.OB.)

Research article, neuroscience

Keywords: TurboID, AII amacrine cell, Electrical Synapse, Connexin 36

The authors declare no competing interests.

Abstract

Electrical synapses containing Connexin 36 (Cx36) represent the main means for direct electrical communication among neurons in the mammalian nervous system. However, little is known about the protein complexes that constitute these synapses. In the present study, we applied different BioID strategies to screen the interactomes of Connexin 36 and its zebrafish orthologue Cx35b in retinal neurons. For *in vivo* proximity labeling in mice, we took advantage of the Cx36-EGFP strain and expressed a GFP-nanobody-TurboID fusion construct selectively in AII amacrine cells. For *in vivo* BioID in zebrafish, we generated a transgenic line expressing a Cx35b-TurboID fusion under control of the Cx35b promoter. Both strategies allowed us to capture a plethora of molecules that were associated with electrical synapses and showed a high degree of evolutionary conservation in the proteomes of both species. Besides known interactors of Cx36 such as ZO-1 and ZO-2 we have identified more than 50 new proteins, such as scaffold proteins, adhesion molecules and regulators of the cytoskeleton. Moreover, we determined the subcellular localization of these proteins in mouse retina and tested potential binding interactions with Cx36. Amongst these new interactors, we identified signal induced proliferation associated 1 like 3 (SIPA1L3), a protein that has been implicated in cell junction formation and cell polarity, as a new scaffold of electrical

synapses. Interestingly, SIPA1L3 was able to interact with ZO-1, ZO-2 and Cx36, suggesting a pivotal role in electrical synapse function. In summary, our study provides the first detailed view of the electrical synapse proteome in retinal neurons, which is likely to apply to electrical synapses elsewhere.

Introduction

With the discovery of acetylcholine as the first neurotransmitter at the beginning of the 20th century, it was widely accepted that chemical synaptic transmission is the only means of communication for neurons. Decades later, several authors independently demonstrated evidence for the existence of electrical synapses in invertebrates as well as in vertebrates, and subsequent studies identified gap junctions, which are composed of clusters of intercellular channels, as the morphological substrates of these synapses (1, 2). Today it is considered common knowledge among neuroscientists that both types of synapses coexist in the nervous system and that each of them provides unique features essential for accurate signal processing. Yet, compared to the efforts that have been made to study protein complexes underlying chemical synapse function and regulation, we know fairly little about the proteome that constitutes an electrical synapse (3).

In contrast to chemical synapses, electrical synapses don't rely on neurotransmitters and specific receptor molecules but instead make use of intercellular channels to convey neural signals bidirectionally in the form of ionic currents (4). This seemingly simple mode of communication allows for an instantaneous signal transmission that synchronizes the activities of electrically coupled neurons giving rise to complex brain functions such as network oscillation, hormone secretion or coordination of motor functions (5, 6).

In the mammalian nervous system, electrical synapses are mainly, but not exclusively formed by Connexin 36 (Cx36), a connexin isoform that is highly specific for neurons (7-9) and often referred to as the "major neuronal connexin". One exception to the rule are the insulin producing beta cells in the pancreas (10). In general, Cx36 gap junction channels are known to exhibit a very low single channel conductance (11) but a remarkable degree of plasticity that allows neurons to regulate the number of open channels and hence the strength of synaptic transmission in order to adapt to environmental stimuli (12). A prime example of a neuron that is heavily coupled via Cx36 and in which the signal transduction pathways that regulate electrical coupling have been well described is the AII amacrine cell (13-15). The AII cell is a glycinergic interneuron in the mammalian retina that is electrically coupled to neighboring AII amacrine cells and to ON Cone

77 bipolar cells (16). The main task of this cell is to collect neural signals that originate in rods and
78 relay them into the cone pathway. This circuit is referred to as the primary rod pathway and it
79 forms the neurophysiological basis for scotopic vision. Within the primary rod pathway, electrical
80 coupling of AII amacrine cells is regulated in an activity dependent manner (13). The opening of
81 Cx36 channels in AII amacrine cells requires the activation of calcium calmodulin dependent
82 kinase II (CaMKII), which is triggered by the influx of calcium through non-synaptic NMDA
83 receptors. Once CaMKII is activated, it binds to Cx36 and phosphorylates the intracellular
84 domains causing the channel to open (13, 17, 18). These activity driven changes clearly resemble
85 long-term potentiation as it has been described for chemical synapses in hippocampal neurons
86 (19). Another, almost obvious, but not less important, parallel between electrical and chemical
87 synapses, is the their basic "architecture": 1) Glutamate receptors, for instance, interact with
88 PSD95 (20), a membrane associated guanylate kinase (MAGUK) that is similar in function and
89 domain structure to ZO-1, another MAGUK and well-known interactor of Cx36. 2) Electrical
90 synapses are surrounded by adhesions (21). 3) As described for glutamatergic synapses,
91 electrical synapses also harbor electron dense structures that appear to consist of a dense
92 assemblage of synaptic proteins (22, 23). However, the composition of this density or the type of
93 adhesion molecule that is necessary to specify where an electrical synapse is formed still remain
94 a mystery and require sophisticated proteomics to solve.
95
96 The task of identifying compartment specific proteomes or interactomes for a given protein of
97 interest (POI) with standard techniques has always been challenging due to the abundance of
98 non-specific background and the requirement to preserve intact protein complexes. To overcome
99 these limitations, several laboratories have developed novel proximity techniques such as
100 TurboID (24, 25), which utilize promiscuous biotin ligases to biotinylate neighboring proteins within
101 a radius of 5 nm of the POI. Like any other tag, TurboID can be fused to the POI and is then
102 expressed in cells, where it is allowed to biotinylate proximal proteins that are subsequently
103 isolated with streptavidin beads under stringent buffer conditions. The ability to directly label
104 "associated" proteins with an affinity tag combined with the fast enzyme kinetics have made
105 TurboID a valuable tool for modern *in vivo* proteomics. Previously, BioID and TurboID have been
106 used to study the proteomes of chemical synapses and even contact sites of astrocytes and
107 neurons in nematodes and mice (26-28).
108
109 In the present study, we have applied two different TurboID approaches to uncover the
110 electrical synapse proteome in the mouse and the zebrafish retina. Contrasting these two

model organisms allowed us to expose essential components of the molecular architecture of vertebrate electrical synapses. Beyond known components of electrical synapses, such as ZO-1 and ZO-2, our screen identified a plethora of new molecules that were not previously shown to associate with Cx36/Cx35b. These include components of the endocytic machinery, adhesion molecules, regulators of the cytoskeleton, membrane trafficking, as well chemical synapse proteins. Overall, our screen showed that many components of electrical synapses in zebrafish and mouse retinas were highly conserved, in particular the ZO proteins and the endocytosis components, indicating a high degree of evolutionary conservation that suggests a critical functional role for these proteins.

Results

Two TurboID approaches allow a glimpse at the electrical synapse proteome in zebrafish photoreceptors and AII amacrine cells of the mouse retina.

In this study, we have adopted two *in vivo* BioID approaches to gain a more comprehensive understanding of protein complexes that are associated with the neuronal connexin Cx36 and its zebrafish orthologue Cx35b in retinal neurons. To implement BioID in zebrafish, we generated a transgenic line expressing a Cx35b-V5-TurboID fusion protein (we used an internal insertion site as previously described (29)) under the control of Cx35b promoter (Figure 1 A). As shown in control experiments, the expression of this construct recapitulated the expression pattern of wildtype Cx35b in photoreceptors (30) which were labelled with ZPR1, indicating that Cx35b-V5-TurboID is correctly targeted to synapses (Figure 1B). The inner retina, however, displayed much weaker expression of the fusion construct, which is why we anticipated that most of the candidates we detected with this strategy are proteins that are associated with Cx35b in photoreceptors. To induce efficient biotinylation in zebrafish we injected 10mM biotin solution intraperitoneally on three consecutive days and isolated biotinylated proteins for mass spectrometry (Figure 1B and C). For the analysis of mass spec data sets we compared the abundance of candidate proteins from the Cx35b-V5-TurboID strain to wildtype samples that did not express TurboID. In Cx35b-V5-TurboID samples, but not in wild type retinas, we found several known interactors of the Gjd2 family such as scaffold proteins including Tjp1a, Tjp1b, Tjp2a, Tjp2b, Mupp1, Psd95 and Af6 (Figure 1D) (31-34). In addition to these candidates, we identified proteins that are involved in membrane trafficking including Syt4, Sec22B, components of the endosomal trafficking machinery Snap91 and Eps15l1a, and an additional Cx36 orthologue termed Cx34.7, which has

145 previously been localized to photoreceptors in bass retina (35). The detection of this Gjd1 isoform
146 via BioID was somewhat surprising, as Cx34.7 was shown to form gap junctions that are
147 separated from Cx35b containing clusters in bass photoreceptors. To determine the subcellular
148 localization of Cx34.7 and its connection to Cx35b in zebrafish photoreceptors, we generated a
149 transgenic Cx34.7-GFP strain, that expressed an internally GFP-tagged fusion protein under the
150 control of the Cx34.7 promoter. In this strain, we found that Cx34.7 was only expressed in the
151 outer plexiform layer (OPL) where it was associated with Cx35b at some gap junctions (Figure
152 1E). Thus, besides known interactors of the Gjd family, our *in vivo* BioID approach identified an
153 additional connexin isoform that is connected to Cx35b in photoreceptors.
154
155 To unravel the Cx36 interactome in the mouse retina we initially delivered a Cx36-V5-TurboID
156 fusion via intravitreal AAV injections into retinal neurons. This construct was similarly designed to
157 the Cx35b clone but regulated by a short human synapsin promoter to drive expression in the
158 neural retina (Figure 2A). Unfortunately, this strategy produced massive overexpression artefacts
159 and resulted in an accumulation of Cx36-V5-TurboID in ganglion cell somas, which would have
160 made an interactome analysis of a synaptic protein impossible. To solve this issue and to ensure
161 that TurboID is targeting electrical synapses, we took advantage of the GFP-directed TurboID
162 approach (36) and the Cx36-EGFP transgenic mouse strain (37-39). The GFP-directed TurboID
163 strategy was initially developed as a modular system for zebrafish by Xiong et al., and utilizes and
164 a destabilized GFP nanobody that is fused to TurboID (36) to direct the biotin ligase towards a
165 given protein of interest carrying a GFP-Tag. To further increase the specificity of our approach
166 and identify the Cx36 interactome within a single type of inhibitory interneuron, the AII amacrine
167 cell, we expressed V5-TurboID-dGBP under control of the HKamac promoter (40). As shown
168 previously, in retinas that were infected with AAVs carrying an HKamac GFP vector, we observed
169 GFP expression mainly in AII amacrine cells but not in bipolar cells (Figure 2B, lack of GFP
170 expression in SCGN labelled neurons). In our hands, we also observed GFP labeling in horizontal
171 cells, which was neglectable for our paradigm, since these neurons do not express Cx36 (41) and
172 because dGBP is degraded unless it is bound to GFP (42). In an initial experiment we injected
173 AAVs carrying HKamac_V5-TurboID-dGBP intravitreally into Cx36-EGFP mice and tracked the
174 localization of the construct two weeks post injection. As expected, all V5 labeled puncta
175 colocalized with Cx36-EGFP, indicating that V5-TurboID-dGBP reached electrical synapses in AII
176 amacrine cells. In the next experiment, we injected a 5 mM biotin solution subcutaneously on 4
177 consecutive days, 3 1/2 weeks post infection. This treatment was sufficient to induce efficient
178 biotinylation (Figure 1B, lower panel and C), and allowed us to capture a plethora of molecules

that were associated with Cx36. To distinguish these proteins from background, we included wild type mice injected with AAV HKamac_V5-TurboID-dGBP throughout the entire experiment and compared the abundance of all proteins we detected. A mass spec hit that was three times or even more abundant in the Cx36-EGFP condition was considered a candidate that is likely to be associated with Cx36. We illustrated the relationship of all proteins that fell into this category in a string diagram (Figure 2D). Among the most abundant proteins in our screen, we identified the ZO proteins ZO-1 and ZO-2 and signal induced proliferation associated 1 like 3 (Sipa1l3), a PDZ domain containing protein that has been implicated in the regulation of cell adhesion and cell polarity. In addition to these candidates, we also identified proteins that are involved in endocytosis, membrane trafficking, regulation of the cytoskeleton, cell adhesion and chemical synapses. All of these hits covered different functional categories of proteins that have been related to connexins (43-48) and thus appear to represent an authentic interactome for a neuronal gap junction protein.

Localization of BioID hits at Cx36 containing gap junctions in the AII amacrine cell

In the next set of experiments, we validated the most abundant candidates from our list in GFP expressing AII amacrine cells. We categorized the proteins based on the cell biological function they serve. In line with the mass spec data, we observed the most frequent colocalization for Cx36 with scaffold proteins including ZO-1, ZO-2, Cingulin and SIPA1L3 (Figure 3A, arrows). Although ZO-1, ZO-2 and cingulin are known components of electrical synapses (34, 44), SIPA1l3 has not been shown before to associate with Cx36, yet it colocalized with the connexin to a similar extent as the ZO proteins, suggesting that it could be essential for synapse formation or stabilization. In addition to scaffolding proteins, we confirmed an association with several adapter proteins of the endocytic machinery, including EPS15L1, SNAP91, HIP1R and ITSN1 (Figure 3B, arrows). In comparison to the scaffold proteins, however, the colocalization of Cx36 with each of these endocytic components, was clearly less frequent and more heterogenous, which appears to reflect different stages in the life cycle of Cx36. Besides synaptic scaffolds and endocytic adapter proteins we tested a variety of additional hits, which include synaptojanin 2 binding protein (Sj2bp), synaptotagmin 4 (categorized as “trafficking”) and several proteins that regulate actin dynamics such as G-protein regulated inducer of neurite outgrowth 1 (Gprin1), dedicator of cytokinesis 7 (Dock7) and microtubule associated protein 6 (Map6). All of these proteins showed considerable colocalization with Cx36 in AII amacrine cell dendrites (Figure 4A, B). We also tested components of chemical synapses including GluR2-3, the scaffold Shank2 (Figure 4D) and Bai1

213 (Figure 4C) a synaptic adhesion molecule implicated in excitatory synapse formation (49). We
214 found that these proteins showed a partial overlap with Cx36 at the periphery of each junction.
215
216 **Identification of novel Cx36 binding partners**
217
218 Thus far, we have gained significant insight into the Cx36 interactome and identified several new
219 molecules as components of electrical synapses in AII amacrine cells. To understand how these
220 molecules are organized at the synapse we tested protein-protein interactions in co-transfected
221 HEK293T cells. Interestingly, two of the novel proteins we detected in AII cells contain PDZ
222 domains and thus may directly bind to Cx36 like ZO-1 and ZO-2 (Figure 5B, GFP-Trap IP with
223 both ZO proteins served as a positive control); these proteins are Sipa1l3 and Sj2bp. We found
224 that Myc-Sipa1l3 interacted with all major components of electrical synapses: ZO-1, ZO-2 and
225 Cx36 in co-transfected HEK293T cells. The overlap of SIPA1L3 and the ZO proteins was confined
226 to cell cortices and to actin like fibers in the cytoplasm (Figure 5A). Additionally, we performed IP
227 experiments and demonstrated that Cx36 binds to Sipa1l3 in a PDZ dependent manner. A
228 truncated version of Cx36 lacking the PDZ binding motif (Cx36/S318Ter) failed to interact with
229 Sipa1l3 in IP experiments. In co-transfected cells we observed that Sj2bp, which contains a single
230 PDZ domain and a transmembrane domain (50), colocalized with Cx36 but not with the
231 Cx36/S318Ter, indicating that the interaction of these proteins requires the PDZ domain. In IP
232 experiments using FLAG tagged Sj2bp as a bait we were unable to coprecipitate Cx36, which
233 was rather surprising as both proteins clearly colocalized in co-transfected HEK293T cells. One
234 possible explanation for the lack of a detectable interaction, is that Sj2bp displays a low affinity
235 for the PDZ binding motif (PBM) of Cx36, as it is the case for ZO-1 (45). We have previously
236 shown that binding of Cx36 to ZO-1 can be artificially enhanced by a simple deletion of amino
237 acids 313-319 within the C-terminus creating a new PBM with the following sequence: RTYV (51).
238 We repeated the IP with this mutant and observed substantial binding to FLAG-Sj2bp (Figure 5B),
239 suggesting that Cx36 and SJ2BP are compatible interactors. In addition to the candidates we
240 overexpressed to verify direct binding interactions, we found that Cx36 colocalized with several
241 endogenous HEK293T proteins that also occurred in our AII cell specific data set, including
242 Eps15l1, Gprin1 and Sec22b (Figure 5C).
243
244
245

246 **Molecular architecture of the AII amacrine cell/On cone bipolar cell gap junction.**

247

248 AII amacrine cells form two different sets of gap junctions, with neighboring AII amacrine cells and
249 with ON cone bipolar cells to convey neural signals that originate in rod photoceptors into the
250 cone pathway (Illustrated in figure 6A) (9). Ultrastructural studies have revealed an asymmetry in
251 the cytoplasm of AII/ON cone bipolar cell junctions (AII/ONCBC), which exhibits an electron dense
252 structure (termed fluffy material) in the AII amacrine cell but not in the cone bipolar cell, hinting at
253 differences in the molecular composition of both sites of the synapse (23, 52). Moreover, apart
254 from accessory proteins that bind to the channel, AII/ONCBC gap junctions are likely to be distinct
255 from AII/AII gap junctions since they recognize ON cone bipolar cells as the correct synaptic
256 partner. These two characteristics of the AII/ONCBC gap junction can only be explained by a
257 unique composition of the synapse proteome. We reasoned that the electron density in the AII
258 cell could harbor several proteins we identified in this study. To test this hypothesis, we triple
259 labelled AAV/HKamac_GFP infected retinas with Scgn, Cx36 and the main candidates from our
260 screen. With this strategy it was possible for us to visualize AII/ONCBC contacts (Figure 6 D,
261 arrows) and the precise localization of each candidate. To illustrate the localization of AII/ONCBC
262 gap junctions in a comprehensive way, we reconstructed the morphology of AII amacrine cells
263 using serial section transmission EM imaging. As seen in figure 6B, most AII/ONCBC gap
264 junctions (shown in yellow) were located above homologous AII/AII contacts (Cyan) and contained
265 electron densities on both sides (Figure 6C).

266

267 The scaffold proteins ZO-1, ZO-2, Cgn and Sipa1l3 localized at AII/ONCBC contacts suggesting
268 that they are a part of the electron density in AII cells (Figure 6D, arrows). In addition to these
269 proteins, we also confirmed that AII/Cone bipolar cell gap junctions contained Syt4, Eps15l1,
270 Sj2bp and Gprin1. Finally, we addressed at the exact localization of the G protein coupled
271 adhesion receptor Bai1, a synaptic adhesion molecule that has been implicated in excitatory
272 synapse formation (49). Interestingly, we observed Bai1 at AII/ONCBC contacts, in the vicinity of
273 Cx36, which is consistent with the notion of synaptic adhesion molecules as an integral part of
274 electrical synapses (21, 53). This finding further implies that Bai1 might play a role in the formation
275 of AII/ONCBC contacts. However, further knock-out studies will be necessary to address the
276 concrete function of this adhesion molecule. Finally, we addressed the subcellular distribution of
277 Sipa1l3 at AII/ONBC gap junctions. We noticed that these junctions often displayed a ring like
278 shape, that contained Sipa1l3 in the center of each ring (Figure 6D). One possible interpretation

279 of this distinct sub-synaptic distribution is that Sipa1l3 is interacting with a type of adhesion
280 molecule that is directly adjacent to the gap junction.
281
282
283 **Electrical synapse scaffolds are targeted to AII amacrine cell/ ON cone bipolar cell contacts**
284 **in the absence of Cx36.**
285
286 Previous studies have shown that ZO-1 localizes to neuronal contact sites even in the absence
287 of connexins (33). This finding is consistent with a study by Meyer et al., (2014), who reported
288 that Cx36-EGFP containing gap junctions colocalize with ZO-1 at AII/ONCBC contacts despite a
289 C-terminal tag in the fusion protein that is known to interfere with PDZ domain mediated
290 interactions (38, 51). One possible interpretation of these observations is that ZO-1, a protein with
291 multiple protein-protein interaction domains, is connected to additional components of the gap
292 junction such as adhesion molecules, the actin skeleton or other MAGUKs that retain the scaffold
293 at the synapse. We wondered if a similar principle applies to the scaffold proteins that were
294 identified in this study and tested the localization of ZO-2 and Sipa1l3 in Cx36 KO retinas that
295 were infected with AAV/HKamac_GFP to visualize AII/ONCBC contacts. Here, we observed that
296 ZO-2 and Sipa1l3 showed a similar effect as ZO-1 and still localized to AII/ONCBC contacts in
297 Cx36 KO retinas (Figure 7A-C). Additionally, we quantified the density and size of immunoreactive
298 Sipa1l3 and ZO-1 in the inner plexiform layer of WT and Cx36 KO mouse retina. While the size
299 of ZO-2 and Sipa1l3 puncta were unchanged in Cx36 KO mice, the density of both ZO-2 and
300 Sipa1l3 puncta were reduced and the colocalization of ZO-2 and Sipa1l3 was reduced in Cx36KO
301 retina. Thus, loss of Cx36 resulted in a quantitative defect in formation of electrical synapse
302 density complexes.
303
304 **Discussion**
305
306 In the present study, we have used TurboID to uncover the electrical synapse proteome in retinal
307 neurons. Our screen identified a plethora of molecules that were associated with the neuronal
308 connexins Cx36/Cx35b in zebrafish and mice such as adhesion molecules, scaffold proteins,
309 chemical synapse proteins, components of the endocytic machinery and cytoskeleton associated
310 proteins (Illustrated in Figure 7 E-F). The presence of ZO proteins and endocytosis components
311 in the Cx36 and the Cx35b interactome data suggests a certain degree of conservation in the

312 proteome of electrical synapses. An apparent difference between species, however, is the
313 existence of additional ZO variants and Cx36 homologues in the zebrafish genome (33), which
314 are also represented in our Cx35b interactome. In contrast to the bass retina, where it was shown
315 that Cx35 and Cx34.7 form two distinct circuits (35), we found that zebrafish photoreceptors
316 formed gap junctions that contained both connexins. Cell culture experiments have confirmed that
317 Cx35 and Cx34.7 are able to form heterotypic channels (54) that exhibit slightly altered voltage
318 sensitivities compared to the homotypic channels. How exactly these gap junction channels in
319 zebrafish photoreceptors are configured and which exact cell types they connect remains to be
320 determined.
321
322 Among other proteins that were detected in this study, we identified Sipa1l3 as a novel scaffold
323 protein for electrical synapses. Interestingly, Sipa1l3 was also described as a component of post
324 synaptic densities of glutamatergic synapses in hippocampal neurons, and is known interact with
325 Fezzins, which occur in a complex with Shank3 (55). Additionally, we found that Sipa1l3 was able
326 to interact with Cx36 and the ZO proteins. This raises the question of what potential function
327 Sipa1l3 might serve given the abundance of colocalization with Cx36 in AII amacrine cells?
328 Genetic screens have shown that mutations in the Sipa1l3 gene result in abnormal eye and lens
329 development and a decrease in the formation of cell adhesions. Like other members of the Sipa1l
330 family, Sipa1l3 also contains a RAP GTPase activating protein (GAP) domain that is known to
331 regulate the activity of RAP proteins, which in the GTP-bound form impacts processes such as
332 adhesion and actin dynamics (56). One way in which Sipa1l3 might influence the formation of
333 electrical synapses might be as a regulator of Rap1 and its effector proteins. To determine the
334 exact function of Sipa1l3 further studies on KO mice will be required.
335
336 One striking aspect of the Cx36 interactome in AII amacrine cells is the abundance of the
337 endocytosis machinery. Considering the short half life time of Cx36 of 3.1 h (29) and the fact that
338 the turnover of electrical synapse proteins is a steady-state process (43), it makes sense that the
339 endocytic machinery is that well represented in our interactome data. Thus, besides
340 phosphorylation, it seems possible that the cellular regulation of turnover mechanisms could
341 function as an additional means to adjust the strength of electrical coupling between AII amacrine
342 cells.
343
344 **Is Bai1 necessary to form electrical synapses in the primary rod pathway?**

How and when it is determined where electrical synapses are formed is currently unknown. It has been suggested that neuronal adhesion molecules serve as cues that wire the correct neurons together (3). This task also has to be accomplished in the primary rod pathway, where AII amacrine cells form synapses among each other and with ON Cone bipolar cells. Interestingly, we identified the brain specific angiogenesis inhibitor 1 (Bai1) between AII amacrine and ON cone bipolar cell gap junctions, which could suggest that Bai1 is necessary to connect these cells. Recent reports have described Bai1 as a synaptogenic enzyme capable of regulating intracellular signaling pathways that determine synapse formation. (49, 57). Thus, besides merely functioning as a cell adhesion molecule, Bai1 might actively support synaptogenesis in AII amacrine cells at a level that is hierarchical to Cx36 and its associated scaffolds, which would explain why these cells form contacts with ON Cone bipolar cells even in the absence of Cx36.

Cell type-specific differences in the Cx36 interactome?

Interestingly, our interactome in AII amacrine cells showed no signs of the scaffolds Mupp1 and Af6, although these candidates were shown to colocalize and interact with Cx36 in mammalian retinas and several other brain regions (31). Moreover, both proteins also showed up in our Cx35b interactome in zebrafish retina. One feasible explanation is that AII cell gap junctions simply lack these scaffolds and that they may instead be used for electrical synapses of other neurons like bipolar cells, which our approach did not consider. In general, it will be interesting to understand how well certain components of the electrical synapse proteome are preserved between cell types. Endocytosis and ZO proteins, for instance, are unlikely to cell-type specific interactors of gap junction channels and are more likely to be ubiquitous constituents of electrical synapses, given their critical function in the constant turnover of Cx36. This is also reflected the evolutionary conservation of these components in the proteomes from zebrafish and mice. Bai1, on the other hand, a protein that is needed to establish specific synaptic contacts, may only occur in certain electrical synapses.

Material and Methods

Animal husbandry of zebrafish

Maintenance and breeding of zebrafish was conducted under standard conditions (58). Wild type (AB) zebrafish were purchased from the Zebrafish International Resource Center (ZIRC, Eugene, OR, USA). Fish were maintained on a 14 h light/10 h dark cycle. All procedures were performed

378 in accordance with the ARVO statement on the use of animals in ophthalmic and vision research
379 and US Public Health Service guidelines and have been reviewed and approved by the
380 Institutional Animal Care and Use Committees at the University of Texas Health Science Center
381 at Houston and the University of Houston.
382
383 **Tol2 mediated transgenesis**
384 Transgenic Cx35b-V5-TurboID fish were generated using the Tol2 system and a donor vector
385 containing 4.5 kb of the Cx35b promoter, exon1 of the Cx35b gene and the open reading frame
386 of Cx35-V5-TurboID. The coding sequence of V5-TurboID (25) was cloned into a region of the
387 Cx35b gene encoding the C-terminal tail. V5-TurboID was inserted between leucine 285 and
388 proline 286 to expose the 19 C-terminal amino acids of Cx35b. Additionally, the donor vector
389 contained a Myl7 promoter driving mCherry expression in the heart to select larvae in which the
390 construct was integrated into genome. Transgenic Cx34.7-oxGFP fish were generated in the
391 same way using a donor vector containing 2.8 kb of the Cx34.7 promoter and the coding sequence
392 of Cx34.7 with oxGFP inserted between aspartate 283 and methionine 284 in the C-terminus. To
393 generate transgenic fish, the donor vector was co-injected with Tol2 transposase mRNA into
394 embryos in the 1 cell stage as described previously (59). Transgenic individuals were raised to
395 adulthood and mated.
396
397 **Animal Husbandry of mice**
398 The experiments in this study were conducted with wildtype mice (C57BL/6J), the Cx36-EGFP
399 strain (37-39) (Kindly provided by Dr. Hannah Monyer) and Cx36 Knock out mice (60) (Kindly
400 provided by Dr. David Paul). Animals of ages 2-12 months were used for experiments. All
401 procedures were performed in accordance with the ARVO statement on the use of animals in
402 ophthalmic and vision research and US Public Health Service guidelines and were approved by
403 the Institutional Animal Care and Use Committee at the University of Houston.
404
405 **AAV constructs and intravitreal injections**
406 All AAV constructs used in this study were generated with the pAAV-9-(5)-hSYN-CAMKII-GFP
407 vector kindly provided by Dr. Neal Waxham. The coding sequence of the AII amacrine cell specific
408 AII promoter Hkamac was previously described by Khabou et al., (2023), and synthesized as a
409 654 base pair gBlocks® fragment by IDT genomics. The hSYN promoter and the coding sequence
410 of CaMKII in the pAAV-9-(5)-hSYN-CAMKII-GFP vector were excised via XbaI and EcoRV and
411 the coding sequence of V5-TurboID-dGBP (36, 51, 61) and GFP were fused to the AII promoter

412 and integrated into the vector via Gibson assembly. Titers of AAV particles for different AAV
413 constructs varied ranging from $8x10^{12}$ to $1x10^{13}$ gc/ml. For each experimental condition similar
414 amounts of virus particles were injected. All virus particles were generated at the Baylor gene
415 vector core facility. All AAV vectors that were used in this study will be made available via
416 Addgene. Prior to each virus injection, mice were anesthetized with 3.5-3.9% isoflurane using the
417 SomnoSuite/Mouse STAT Pulse Oximeter (SS-01-03, Kent Scientific Corporation). Once the
418 animal was anesthetized, a small incision next to the pupil was made using a 30 G needle.
419 Afterwards, 1.5 µl of the virus solution was carefully injected intravitreally. Eyes were collected 2-
420 4 weeks after each experiment.
421

422 **DNA constructs**

423 FLAG-SJ2BP and Myc-SIPA1L3 constructs were used in previous studies (50, 62). Venus-ZO-1
424 (#56394) and GFP-ZO-2 (#27422) were purchased from Addgene. The FLAG-Gprin1 (Clone:
425 OMu09339D) and FLAG-EPS15L1 (Clone: OMu22488D) constructs were purchased from
426 Genscript. All Cx36 pcDNA3.1 expression vectors were generated in previous studies (51, 61,
427 63).
428

429 ***In vivo* Biotinylation**

430 *In vivo biotinylation in zebrafish.* Prior to biotin injections, adult zebrafish were anesthetized with
431 0.02% Tricaine and immobilized in a small wax mold. A small incision was made into the abdomen
432 and 30 µl of a 5mM biotin (solved in PBS) solution was injected intraperitoneally using a Hamilton
433 syringe. This procedure was repeated for 2 consecutive days. Afterwards the fish were sacrificed
434 by a cold shock and the retinas were extracted. The streptavidin pull down was carried out as
435 previously described (51, 61). 80 retinas for each condition (Wild type vs. Cx35b-V5-TurboID)
436 were used.
437 *In vivo biotinylation in mouse.* 3 ½ weeks after intravitreal virus injections mice were anesthetized
438 with isoflurane and 1ml of a 5mM was injected subcutaneously for 4 consecutive days. 17 retinas
439 of each condition (Cx36-EGFP vs. wild type) were used for the streptavidin pull down.
440

441 **Bioinformatics**

442 A ratio of Cx36 conditions to the control was used to identify any proteins that were enriched
443 greater than 3-fold in mouse retina and 2-fold in zebrafish retina. Proteins above this threshold
444 were run through the Cytoscape (V3.10.2) plugin ClueGo (V2.5.10) to identify the GO Biological

445 Processes that were upregulated in each Cx36 condition across both zebrafish and mouse
446 species (64, 65). Pathways that show a p-value of less than 0.05 were used for analysis. To
447 determine protein-protein interaction networks, proteins above threshold were also run through
448 the standard STRING (V12.0) pipeline (66).
449

450 **Cell culture**

451 Human embryonic kidney 293 T cells (HEK293T/17; catalog #CRL-11268; ATCC, Manassas, VA,
452 USA) were grown in Dulbecco's Modified Eagle Medium (DMEM) supplemented with 10% fetal
453 bovine serum (FBS), 1% penicillin and streptomycin, and 1% non-essential amino acids (all
454 Thermo Fisher Scientific, Rockford, IL, USA) at 37 °C in a humidified atmosphere with 5% CO2.
455 For pull-down experiments 1 million cells were plated in 60mm dishes. Transfections were carried
456 out with Geneporter 2 as previously described (51).
457

458 **Immunocytochemistry**

459 Immunolabeling of transfected HEK293T cells was carried out as previously described (61, 63).
460 Transfected HEK293T expressing the proteins of interest were briefly rinsed in PBS and fixed in
461 2% paraformaldehyde (PFA) solved in PBS for 15 min at RT. After the fixation step, the coverslips
462 were washed three times in PBS for 10 min and incubated with the primary antibody solution
463 containing 10% normal donkey serum in 0.5% Triton X-100 in PBS overnight at 4 ºC .The following
464 antibodies were used: mouse anti Cx36, 1:500 (MAB3045, Millipore), rabbit anti SIPA1l3, 1:200
465 (30544-1-AP, Proteintech), anti GFP, 1:250 (A10262, Thermofisher), rabbit anti EPS15L1, 1:250
466 (PA5-65940, Thermofisher) and mouse anti V5, 1:500 (R960-2, Thermofisher), rabbit anti myc
467 (16286-1-AP, Proteintech). At the next day, the coverslips were washed 3x10 min in PBS and
468 incubated with the secondary antibodies diluted in 10% normal donkey serum in 0.5% Triton X-
469 100 in PBS at RT under light protected conditions. The following secondary antibodies were used:
470 from donkey, 1:500, conjugated with Cy3, Alexa488, Alexa568, or Alexa647 (Jackson
471 Immunoresearch, West Grove, PA). Afterwards coverslips were washed 3x10 min in PBS and
472 mounted with Vectashield containing DAPI (H-2000, Vector Laboratories Inc.)
473

474 **Immunohistochemistry**

475 Immunolabeling of vertical sections was carried out as previously described (67, 68). Mice were
476 anesthetized with isoflurane and sacrificed via cervical dislocation. The eyes were removed from
477 the animal and opened with a circular cut around the *ora serrata*. The lens was removed, eyes
478 were fixed with 2% PFA solved in PBS for 20 min at room temperature and washed 3x10 min in

479 PBS. Afterwards eyecups were stored in 30% sucrose at 4ºC overnight. On the next day eyecup
480 preparations were embedded in Tissue-Tek O.C.T. cryomatrix (Sakura Finetek, Torrance, CA,
481 USA) and stored at -20ºC. Eyecups were cut into 20 µm thin section and incubated at 37ºC for
482 30 min. Afterwards the slides were washed with PBS (2x5 min) and incubated in the primary
483 antibody solution containing 10% normal donkey serum in 0.5% Triton X-100 in PBS overnight.
484 The following primary antibodies were used: Cx36, 1:250 (Clone: 8F6, MAB3045, Millipore);
485 Cx36, 1:250 (Clone: 1E5H5, 37-4600, Thermofisher); GFP, 1:250 (A10262, Thermofisher); ZO-1,
486 1:250 (Clone: ZO1-1A12, 33-9100, Thermofisher); ZO-2, 1:250 (71-1400, Thermofisher); CGN,
487 1:250 (PA5-5561, Thermofisher); SIPA1L3, 1:100 (30544-1-AP, Proteintech); EPS15L1, 1:250
488 (PA5-65940, Thermofisher); HIPR1, 1:250 (AB9882,Sigma); GluR2-3, 1:200 (07-598, Sigma);
489 Gprin1, 1:100 (13771-1-AP, Proteintech); DOCK7, 1:100 (13000-1-AP, Proteintech); MAP6, 1:100
490 (NBP2-14220, Novus Biologicals); Synaptotagmin4, 1:100 (105 143, Synaptic Systems); SJ2BP,
491 1:100 (15666-1-AP, Proteintech); BAI1, 1:100 (NB110-81586, Novus Biologicals); SHANK2, 1:500
492 (Synaptic Systems, 162204); SCGN, 1:250 (CSB-PA020821LA01HU, ARP); SCGN, 1:500
493 (RD184120100, Biovendor); Vglut1, 1:500 (AB5905, Sigma); ITNS1, 1:100-250 (PA5-115432,
494 Thermofisher). The next day, the slides were washed 3x10 min and incubated with secondary
495 antibodies diluted in 10% normal donkey serum in 0.5% Triton X-100 in PBS for 1h at RT under
496 light protected conditions. The following secondary antibodies were used: from donkey, 1:250,
497 conjugated with Cy3, Alexa488, Alexa568, or Alexa647 or Dylight 405 (Jackson Immunoresearch,
498 West Grove, PA). Afterwards the slides were washed 3x10 min and mounted with Vectashield (H-
499 1900, Vector Laboratories, Inc.).
500
501 **Immunoprecipitation**
502 Immunoprecipitation experiments were carried out as previously described (46). 1.5 x10^6
503 HEK293T cells were plated on 60mm dishes and co-transfected at the next day with 2 µg of each
504 vector using Geneporter2 (Amsbio) transfection reagent. 24h after transfection, cells were rinsed
505 in phosphate buffered saline (pH 7.4) and transferred to a reaction tube. The cells were
506 centrifuged at 5000g for 5 min and afterwards homogenized in immunoprecipitation buffer (IP
507 buffer) containing 200mM NaCl, 2m EDTA, 1% Tx-100, 50mM Tris HCL (pH 7.5) supplemented
508 with protease inhibitors (Roche) and 1mM DTT. The lysate was sonicated 3x for 30 seconds and
509 incubated on ice for 30 min. Afterwards, the lysate was centrifuged at 10,000g for 10 min. 20 µl
510 of ChromoTek GFP-Trap® agarose beads (gta, Proteintech) were applied to the supernatant and
511 incubated overnight at 4ºC on a rotating platform. The next day the sample was centrifuged at
512 2500g for 5 min and washed three times in IP buffer. Bound proteins were eluted with 60 µl of 1x

513 Laemmli buffer (BioRad, 1610747) for 5 min at 95ºC. IP experiments for Myc-Sipa1l3 and FLAG-
514 Sj2bp were conducted under a slightly modified protocol. For IP experiments with Myc- Sipa1l3
515 0.5 µg of Sipa1l3 antibody (30544-1-AP, Proteintech) was applied to the cell lysate and incubated
516 overnight on a rotating platform. The next day, 40 µl of prewashed protein A/G beads (Pierce)
517 were applied to the cell lysate and incubated for 1h at 4 ºC. Afterwards the beads were washed 3
518 times and bound proteins were eluted with 1x Laemmli buffer. IP experiments with FLAG-Sj2bp
519 were performed with 20 µl ChromoTek DYDDDDK Fab-Trap® (ffa, Proteintech). Prior to the IP
520 cell lysates were centrifuged at 20,000g for 30 min at 4ºC. Afterwards, cell lysates were incubated
521 with agarose overnight and washed 3 times at 4ºC. Bound proteins were eluted with 60 µl of 1x
522 Laemmli buffer.
523
524 **Western blot**
525 Protein samples were separated via SDS-PAGE containing 7.5% (for Sipa1l3 blots) or 10%
526 polyacrylamide. Proteins were transferred to nitrocellulose membranes using the transblot turbo
527 system as previously described (51). Blots were blocked in 5% dried milk powder in TBST (20 mM
528 Tris pH 7.5, 150 mM NaCl, 0.2% Tween 20) for 30 min at RT and incubated overnight in the
529 primary antibodies diluted in blocking solution at 4ºC on a rotating platform. The following primary
530 antibodies were used: Cx36, 1:500 (Clone: 8F6, MAB3045, Millipore); Cx36, 1:500 (Clone:
531 1E5H5, 37-4600, Thermofisher), SIPA1L3, 1:4000 (30544-1-AP, Proteintech), GFP, 1:1000 (2956,
532 Cell Signaling), V5 1:1000 (R960-2, Thermofisher). Biotinylated proteins detected with high
533 sensitivity streptavidin-HRP, 1:1000 (Abcam). At the next day, blots were washed 3x10 min in
534 TBST and incubated with the secondary antibodies, diluted in the blocking solution as described
535 previously (51). The following secondary antibodies were used: goat anti mouse HRP, 1:1000
536 (34130) and goat anti rabbit, 1:1000 (34160, Thermofisher). Afterwards, the blots were washed
537 3x10 min in TBST and incubated with the ECL solution (32106, Thermofisher) for detection. ECL
538 was detected with the Biorad ChemicDoc™ MP Imaging System.
539
540 **Confocal microscopy and image analysis**
541 Fluorescence images were acquired with a confocal laser scanning microscope (Zeiss LSM 800)
542 using a 60x oil objective and the Airy scan function (Pixel size: 50 nm). Confocal scans were
543 processed using Fiji (ImageJ2 version 2.14.0/1.54f) software (69). The threshold was adjusted
544 using the *Triangle* function for the entire z-stack (7 slices; 1.08 µm). Two regions of interest (ROI)
545 with the size of 20.07 x 32.91 μm^2 were positioned to cover the ON and OFF IPL layers. Frequency
546 and size of the immunoreactive puncta were measured for each channel using the “analyze

547 particles" function. Colocalization of ZO-1 and Sipa1l3 was quantified using the *Colocalization*
548 plugin in Fiji. The number of colocalized puncta and the colocalization was measured using the
549 *Analyze* particle function with a size an exclusion criterion of >100^2 pixels. Following the
550 quantification, the size, density and percentage of the colocalized puncta were averaged for each
551 protein.
552
553 **Volume construction**
554 Retinal Connectome 2 (RC2) is an ultrastructural dataset acquired from the retina of a light-
555 adapted 5-month-old female C57BL/6J mouse (70). Methods concerning tissue acquisition and
556 processing, volume assembly, visualization, and annotation following that extensively detailed for
557 RC1 (71, 72). In short, the RC2 dataset spans the ganglion cell layer through outer nuclear layer
558 of a 0.25 mm-diameter field of retina. RC2 was constructed from 1335 serial TEM sections (70
559 nm thick), captured at 2.18 nm/pixel via Automated Transmission Electron Microscopy at 5000X
560 and combined with 31 optical sections intercalated throughout the volume. These optical sections
561 were probed for small-molecule signals for computational molecular phenotyping (73). Sections
562 were aligned into a single volume using the NCR ToolSet, which has since been replaced by
563 Nornir (RRID:SCR_016458). All protocols were in accord with Institutional Animal Care and Use
564 protocols of the University of Utah, the ARVO Statement for the Use of Animals in Ophthalmic
565 and Visual Research, and the Policies on the Use of Animals and Humans in Neuroscience
566 Research of the Society for Neuroscience.
567
568 **Statistical analysis**
569 Data sets acquired in this study were analyzed with GraphPad Prism 8. Data are shown as
570 mean ± SEM. Normality was tested using the Anderson–Darling and the D'Agostino-Pearson test.
571 Significance was tested using the two-tailed Mann–Whitney U test. For multiple comparisons a
572 one-way ANOVA was performed.
573
574 **Acknowledgements**
575 This project was supported by NIH grants R01EY012857 (J.O.), RF1MH120016 (A.E.P., J.O.),
576 and R21NS085772 (A.E.P., J.O.) and core grant P30EY007551. S.T. was funded by the *Deutsche*
577 *Forschungsgemeinschaft* (DFG) (TE 1459/1-1, Walter Benjamin stipend). E.S. was supported by
578 NIH training grant TL1TR003169 and individual grant F31EY034793. B.W.J. and C.L.S. are
579 supported by NIH grants R01EY028927 (to B.W.J.) and P30EY014800 (to the Moran Eye Center
580 Core); NSF grant 2014862; an Unrestricted Research Grant from Research to Prevent Blindness,
581 New York, NY to the Department of Ophthalmology & Visual Sciences, University of Utah; and an
582 Unrestricted Research Grant from Gabe Newell (to B.W.J.). We would like to thank Dr. Adam C.

583 Miller and Dr. Jen Michel for the helpful discussions. We appreciate Nikki Brantley's support in
584 the cell culture lab.
585

586 **Author contributions**

587 S.T and J.O designed the research. S.T, E.S, E.O.A.M.K, H.H, F.A.E, C.L.S, Y.P.L and K.D
588 performed experiments. K.E and C.R contributed reagents and analytic tools. S.T wrote the paper.
589 All authors edited the paper.

590

591 **Figure legends**

592

593 **Figure 1: Generation of a Cx35b-V5-TurboID zebrafish line. (A)** Cartoon illustrating the
594 generation of Cx35-V5-TurboID fish via Tol2-mediated transgenesis and outline of *in vivo*
595 biotinylation experiments. To induce efficient proximity labeling, zebrafish were intraperitoneally
596 injected with 30µl of 5mM biotin (PBS) for three consecutive days. Afterwards the animals were
597 sacrificed, and the retinas were isolated for streptavidin pull-downs. **(B)** Confocal scans of entire
598 zebrafish retinas, the outer retina including ZPR1 labeled photoreceptors to confirm successful
599 targeting of Cx35b-V5-TurboID to photoreceptor gap junctions. Neutravidin Oregon Green
600 labeling was used to validate efficient proximity biotinylation of Cx35b and surrounding molecules
601 in biotin injected Cx35b-V5-TurboID fish. Reagent or antibody used for labeling is shown in the
602 gray box above each image. Scale 10µm. **(C)** Western blot of streptavidin pull-downs probed with
603 V5 antibodies and streptavidin-HRP. The arrows indicate the position of the Cx35-V5-TurboID
604 construct, which is detected with streptavidin-HRP and a V5 antibody. **(D)** String diagram
605 illustrating the protein-protein network surrounding Cx35b. Proteins that were two times or more
606 abundant in comparison to the control condition were included in the string diagram. **(E)**
607 Colocalization of Cx35b and Cx34.7-GFP in the outer plexiform layer of the zebrafish retina
608 suggests that a subset of photoreceptor gap junctions contain both connexins. Scale: 5 µm; inset
609 scale: 0.5 µm.

610

611 **Figure 2: A GFP-directed TurboID approach uncovers the Cx36 interactome in AII amacrine**
612 **cells. (A)** Cartoon illustrating different *in vivo* BioID approaches used to target Cx36. In strategy
613 1 we expressed an AAV Cx36-V5-TurboID construct with an internal insertion site under the
614 control of the human synapsin promoter. This strategy greatly resulted in overexpression artefacts
615 causing aberrant protein localization. In strategy 2 we adapted the GFP-directed TurboID strategy
616 developed by Xiong et al., (36) to shuttle a V5-dGBP-TurboID construct to Cx36-EGFP containing
617 gap junctions in retinas of the Cx36-EGFP transgenic strain. **(B)** Vertical sections of AAV infected

618 retinas confirming cell type-specificity of our AAV vectors. The HKamac promoter developed by
619 Khabou et al. (40) is mainly active in AII amacrine cells, and does not show any expression in
620 bipolar cells (SCGN, magenta). V5-dGBP-TurboID colocalizes with Cx36-EGFP in AAV
621 transduced retinas, confirming the successful delivery of TurboID to the gap junction. Scale: 5µm.
622 **(C)** Western blot confirming successful biotinylation and capture of Cx36-EGFP, biotinylated
623 proteins and V5-TurboID-dGBP. **(D)** String diagram illustrating the protein-protein interaction
624 network associated with Cx36 in AII amacrine cells. Proteins that were three times or more
625 abundant compared to the control condition were included in the string diagram.
626
627 **Figure 3: Localization of scaffold and endocytosis proteins identified by BioID at Cx36 gap**
628 **junctions in AAV transduced AII amacrine cells expressing GFP. (A)** Colocalization of Cx36
629 and scaffold proteins including known interactors such as ZO-1, ZO-2 and cingulin. Besides these
630 known interactors, we identified Sipa1l3, a PDZ domain containing protein implicated in cell
631 adhesion and cytoskeletal organization. Sipa1l3 shows abundant colocalization with Cx36. **(B)**
632 Colocalization of Cx36 and components of the endocytosis machinery. Among all proteins we
633 have tested, we found frequent colocalization for EpsS15l1, an endocytic adapter protein, and
634 Cx36. Scale: 10 µm. Magnified inset: 1 µm.
635
636 **Figure 4: Localization of trafficking, cytoskeleton-associated, adhesion and synaptic**
637 **proteins identified by BioID at Cx36 gap junctions in AAV transduced AII amacrine cells**
638 **expressing GFP. (A)** Proteins implicated in membrane trafficking Sj2bp and Syt4 colocalize with
639 Cx36 in AII amacrine cells. **(B)** Several cytoskeleton associated proteins and regulators such as
640 Map6, Dock7 or Gprin1 colocalize with Cx36 in AII cell dendrites. **(C)** The adhesion molecule Bai1
641 was often colocalized with Cx36 in AII cell dendrites. **(D)** Often components of chemical synapses
642 such as Shank2 and Glur2-3 were found in the periphery of gap junction plaques in AII amacrine
643 cells. Scale: 10 µm. Magnified inset: 1 µm.
644
645 **Figure 5: Sipa1l3, Sj2bp and Eps15l1 interact with Cx36. (A)** Coexpression of Sipa1l3 with
646 ZO-1, ZO-2 and Cx36. In transfected HEK293T cells Sipa1l3 colocalizes with all three proteins.
647 Colocalization of Sj2bp with Cx36 but not with a Cx36 mutant that lacks the PDZ binding motif.
648 **(B)** Domain organization of constructs used for IP experiments. Co-precipitation of Cx36 and
649 Sjbp2 and SipaA1l3 from lysates of co-transfected HEK293T cells. The PDZ binding deficient
650 Cx36/S318Ter fails to bind Sjbp2 and Sipa1l3. IP experiments with ZO-1 and ZO-2 serve as a
651 positive control. The proteins that were captured in each IP experiment are indicated with arrows

652 in magenta. Cx36 dimers in IP samples are indicated with red arrows and monomers are indicated
653 with blue arrows. **(C)** In transfected HEK293T cells, Cx36 is associated with endogenous proteins
654 that were also detected in AII amacrine cells. Line scans next to each panel illustrate the close
655 association of these proteins (56) with Cx36 (magenta). These proteins were also captured via
656 GFP directed proximity biotinylation. Scale: 10 µm. Magnified inset: 1µm.
657
658 **Figure 6: Localization of BioID "hits" at AII amacrine cell/ON cone bipolar cell junctions.**
659 **(A)** Cartoon illustrating the neurons involved in the primary rod pathway and the subcellular
660 localization of AII/Cone bipolar cell junctions (dashed rectangle). **(B)** 3D reconstruction of AII
661 amacrine cells illustrating the localization of AII-AII gap junctions (cyan plaques in second image)
662 and AII/ON Cone bipolar cell gap junctions (yellow plaques in second image). EM micrographs of
663 AII/On Cone bipolar cell gap junctions. Pseudo colored: Gap junction (Cyan), AII cell (Magenta)
664 and ON cone bipolar cell (Yellow). **(C)** Several of the proteins we identified in AII amacrine cells
665 colocalize with Cx36 at AII/cone bipolar cell junctions. The right plot for each panel depicts an
666 intensity scan of a horizontal region of interest in the middle of each gap junction (arrow). Scale:
667 10 µm. Magnified inset: 1 µm.
668
669 **Figure 7: AII amacrine cell/ON cone bipolar cell contacts remain in Cx36 KO retinas and**
670 **contain electrical synapse scaffolds.** AII amacrine cell/ON cone bipolar cell contacts were
671 visualized with GFP and SCGN. In Cx36 KO retinas, ZO-1, ZO-2 and Sipa1l3 still localize to
672 AII/CBC contacts. **(D)** Both Sipa1l3 and ZO-1 puncta density in the inner plexiform layer were
673 reduced in Cx36KO, but puncta size was unchanged. Colocalization of Sipa1l3 and ZO-1 was
674 reduced in Cx36KO. **(E-F)** Cartoon illustrating Scale: 10 µm. Magnified inset: 1µm.
675
676 **Figure S1: Localization of additional proteins captured with BioID. (A)** Ajm1 labels the base
677 of AII cell somas but does not directly colocalize with Cx36. **(B)** Cap1 is associated with Cx36 in
678 AII cell dendrites. **(C)** Nbea does not directly associate with Cx36 but is often found close Cx36
679 clusters. Scale: 10 µm.
680
681 **Figure S2: Localization of Ncam1 cluster in proximity to Cx36 in AII amacrine cells.** Ncam1
682 labeling does overlap with Cx36 but is found adjacent to gap junctions. Scale**:** 10 µm.

683 **Figures**

684 **Figure 1**

685
686
687
688
689
690
691
692
693
694
695
696
697
698
699
700
701
702
703
704
705
706
707
708
709
710

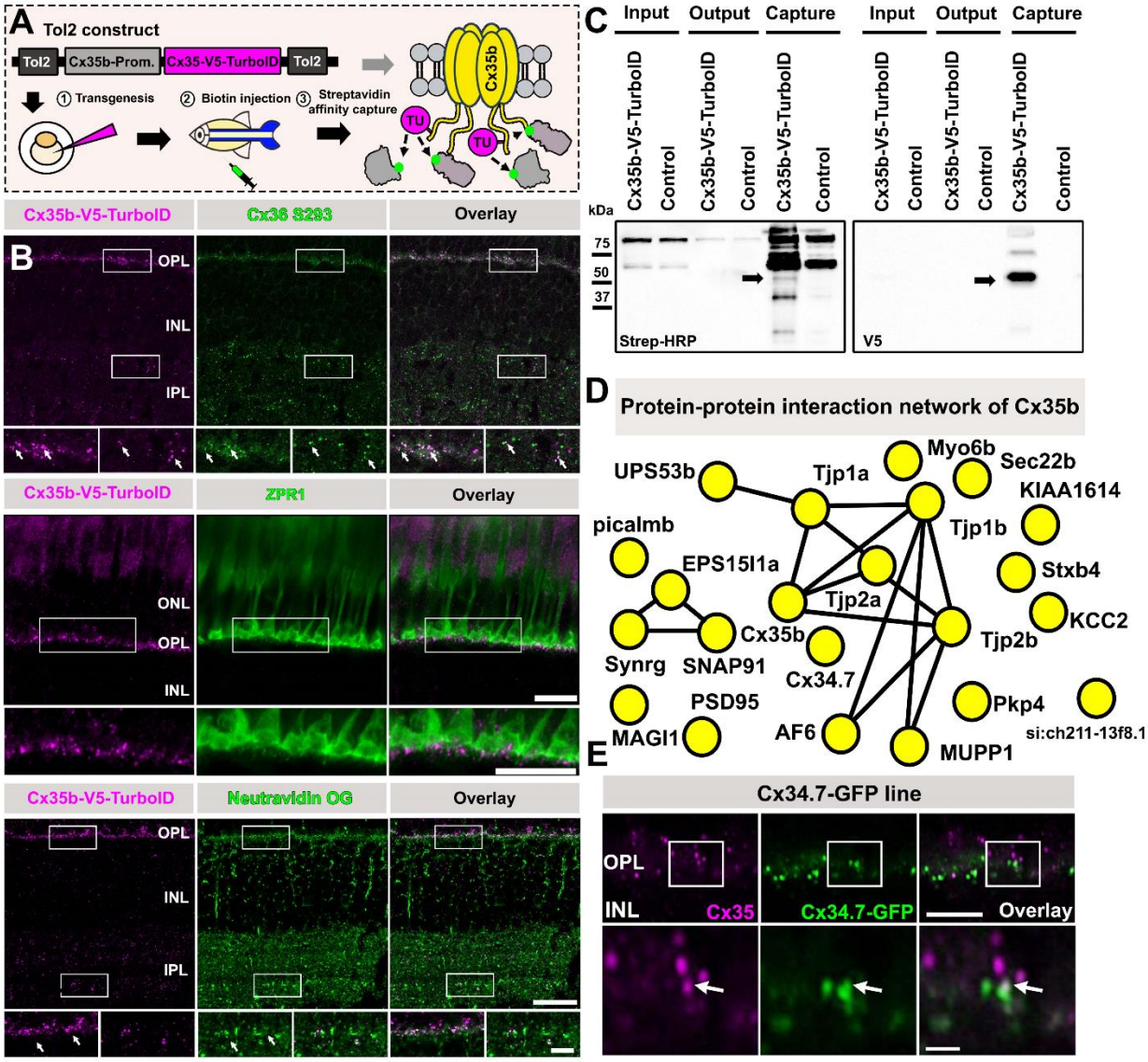

Figure 2

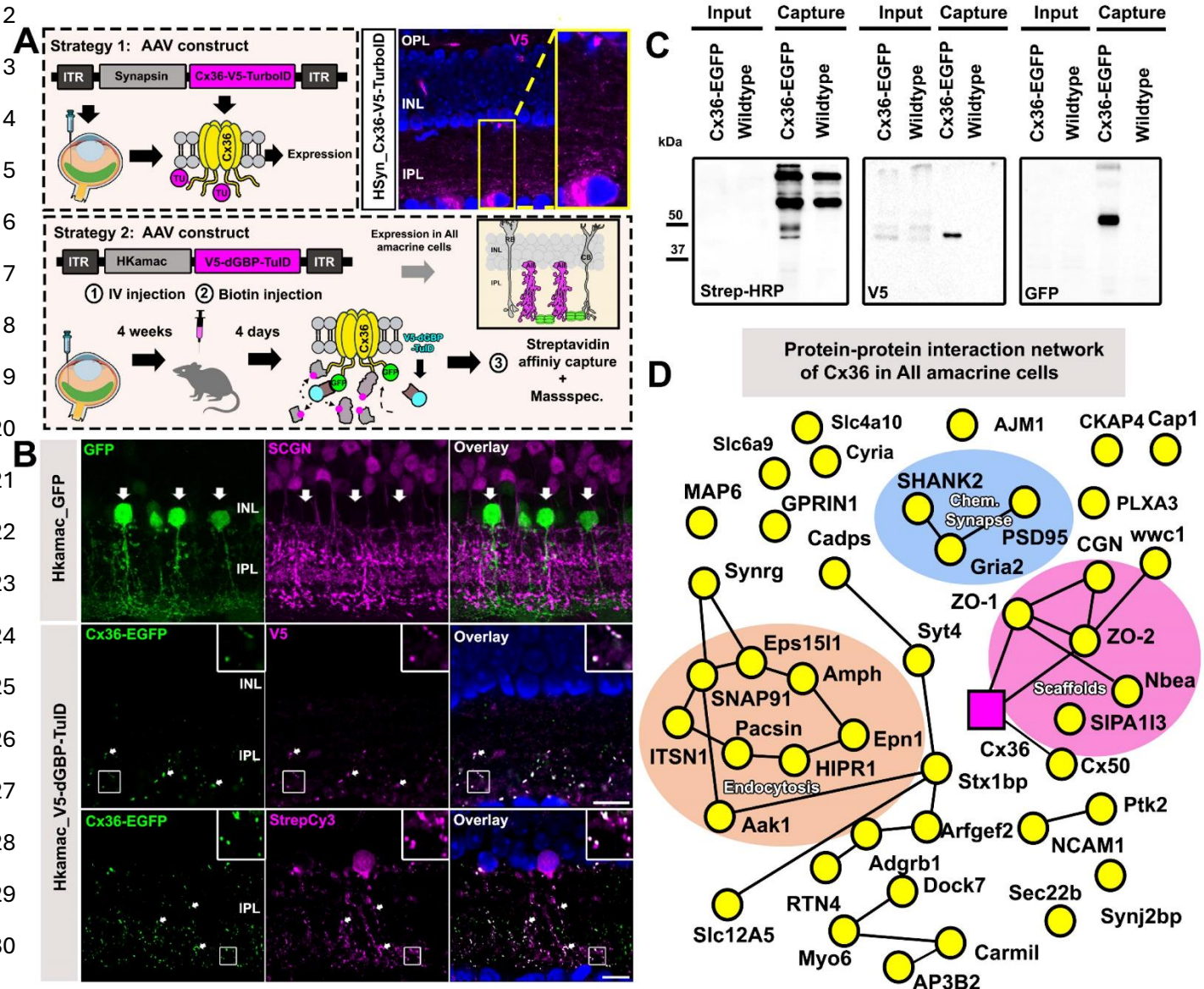
A
Strategy 1: AAV construct
ITR
Synapsin
Cx36-V5-TurboID
ITR
Cx36
Expression
HSyn_Cx36-V5-TurboID
OPL
V5
INL
IPL
Strategy 2: AAV construct
ITR
HKamac
V5-dGBP-TuID
ITR
Expression in All amacrine cells
① IV injection ② Biotin injection
4 weeks
4 days
Cx36
V5-dGBP -TuID
GFP
③ Streptavidin affiniy capture + Massspec.
B
Hkamac_GFP
GFP
SCGN
Overlay
INL
IPL
Hkamac_V5-dGBP-TuID
Cx36-EGFP
V5
Overlay
Cx36-EGFP
StrepCy3
Overlay
C
Input
Capture
Cx36-EGFP
Wildtype
kDa
50
37
Strep-HRP
V5
GFP
D
Protein-protein interaction network of Cx36 in All amacrine cells
Slc4a10
AJM1
CKAP4
Cap1
Slc6a9
Cyria
MAP6
GPRIN1
SHANK2
Chem. Synapse
PSD95
Gria2
PLXA3
Cadps
CGN
wwc1
Synrg
ZO-1
ZO-2
Syt4
Eps15l1
Amph
SNAP91
Scaffolds
Nbea
SIPA1l3
Pacsin
Epn1
ITSN1
HIPR1
Cx36
Cx50
Endocytosis
Stx1bp
Ptk2
Aak1
Arfgef2
NCAM1
Adgrb1
Dock7
Sec22b
RTN4
Synj2bp
Slc12A5
Myo6
Carmil
AP3B2

739 **Figure 3**

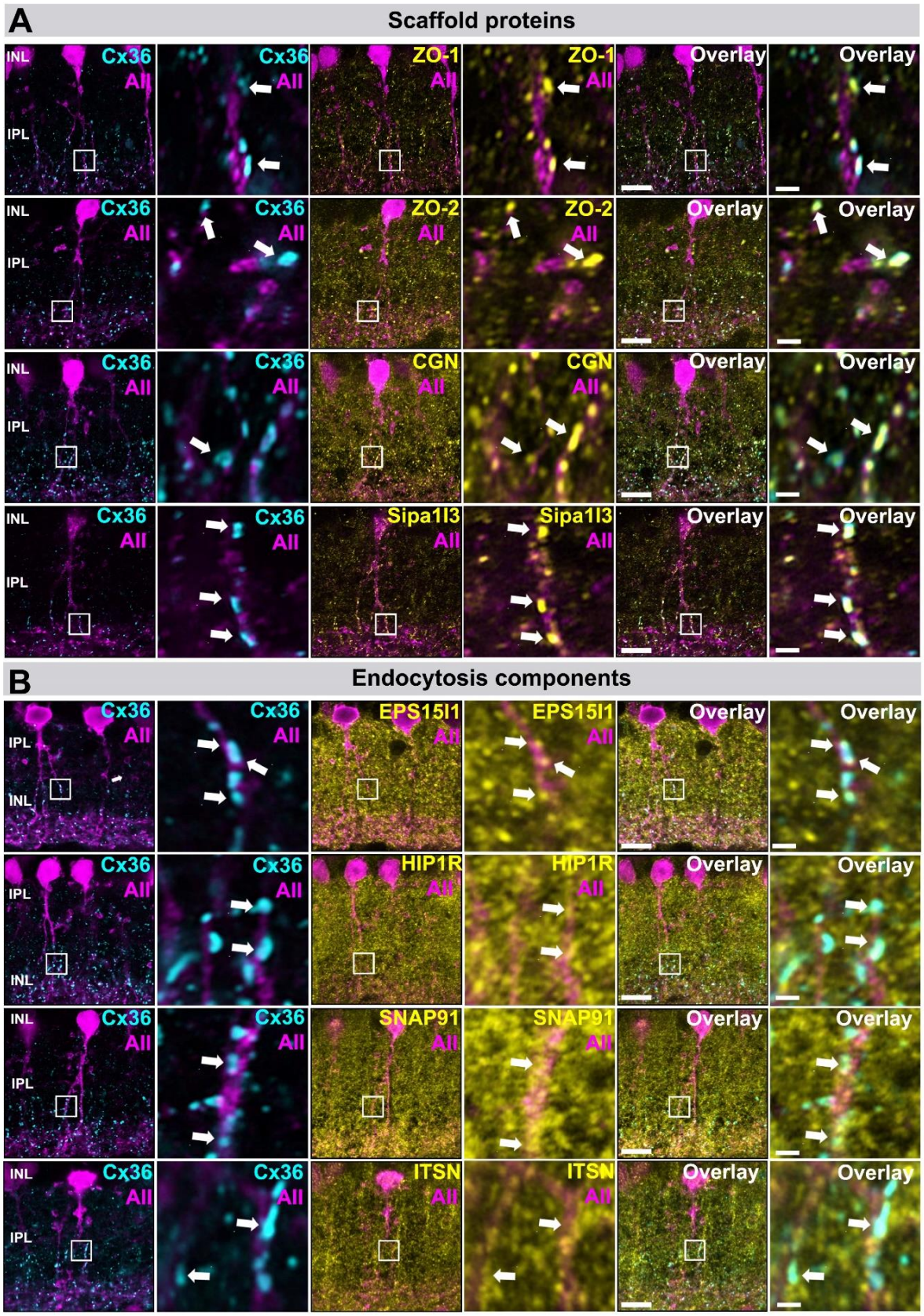
A
Scaffold proteins
INL
IPL
Cx36
AII
ZO-1
ZO-2
CGN
Sipa1l3
Overlay
B
Endocytosis components
EPS15l1
HIP1R
SNAP91
ITSN

767 **Figure 4**

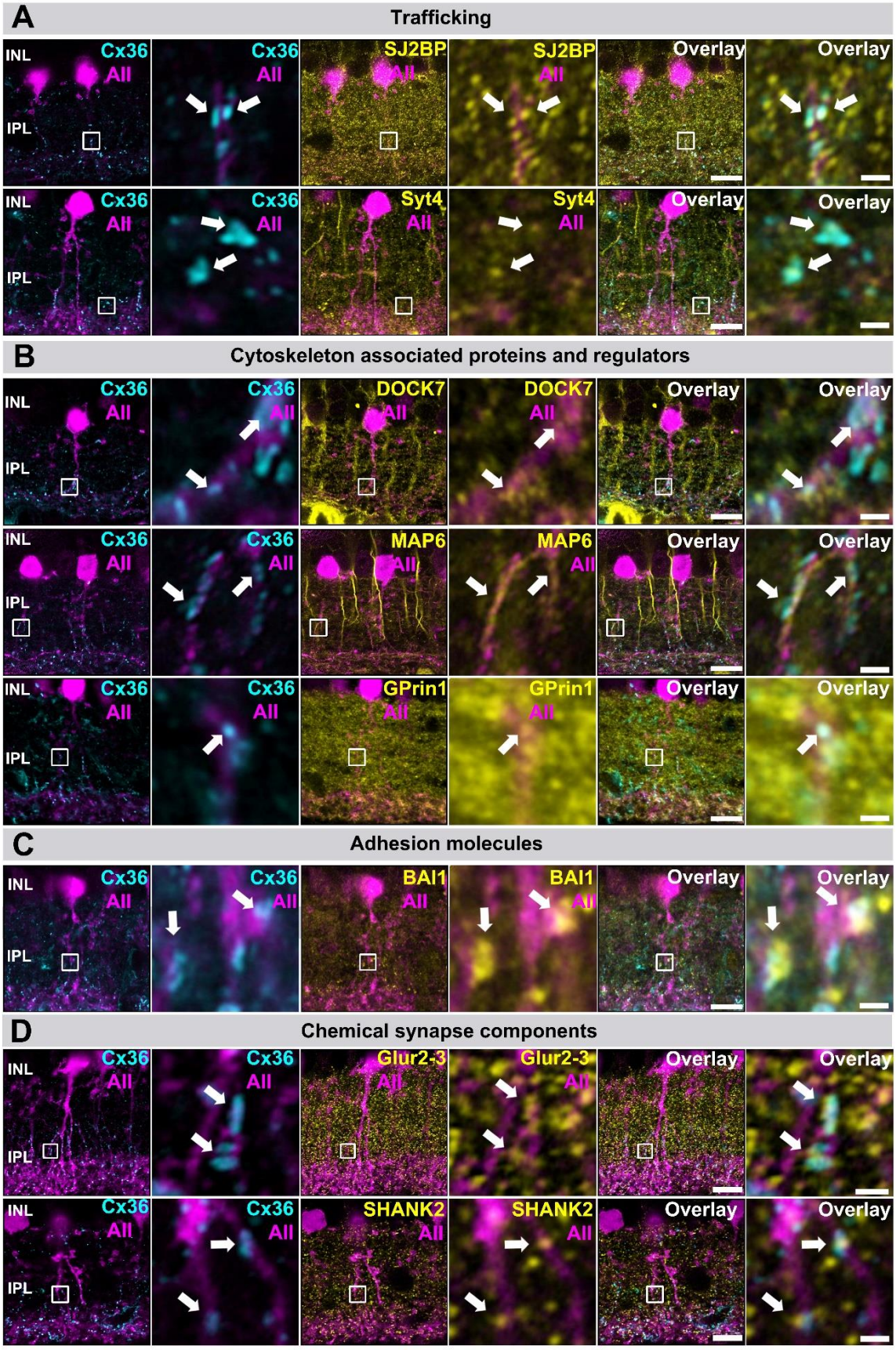

768
769
770
771
772
773
774
775
776
777
778
779
780
781
782
783
784
785
786
787
788
789
790
791
792
793
794

Figure 5

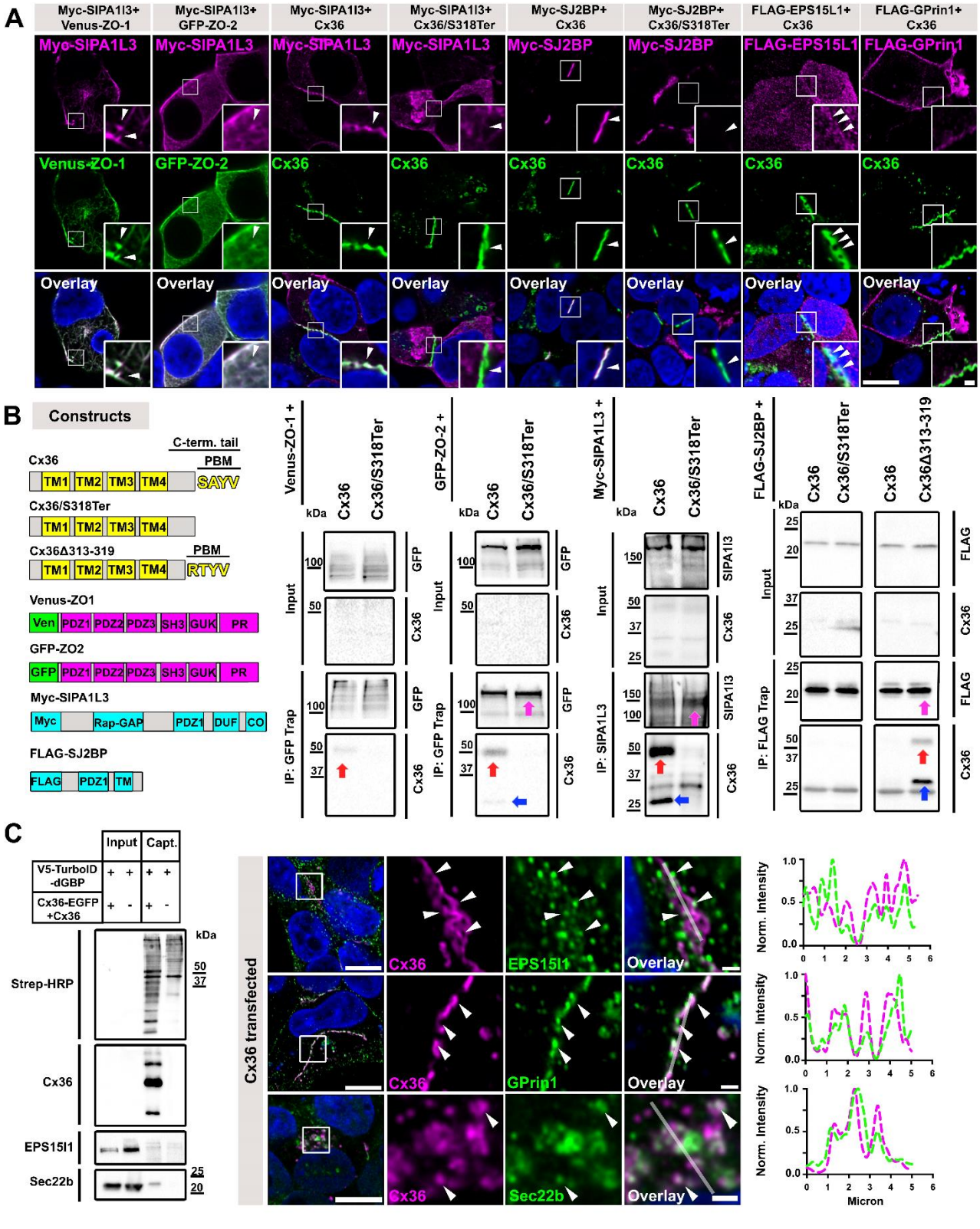
A
Myc-SIPA1l3+ Venus-ZO-1
Myc-SIPA1l3+ GFP-ZO-2
Myc-SIPA1l3+ Cx36
Myc-SIPA1l3+ Cx36/S318Ter
Myc-SJ2BP+ Cx36
Myc-SJ2BP+ Cx36/S318Ter
FLAG-EPS15L1+ Cx36
FLAG-GPrin1+ Cx36
Myc-SIPA1L3
Myc-SJ2BP
FLAG-EPS15L1
FLAG-GPrin1
Venus-ZO-1
GFP-ZO-2
Cx36
Overlay
B
Constructs
C-term. tail
PBM
SAYV
RTYV
TM1
TM2
TM3
TM4
Cx36
Cx36/S318Ter
Cx36Δ313-319
Venus-ZO1
Ven
PDZ1
PDZ2
PDZ3
SH3
GUK
PR
GFP-ZO2
GFP
Myc-SIPA1L3
Myc
Rap-GAP
DUF
CO
FLAG-SJ2BP
FLAG
TM
Venus-ZO-1 +
GFP-ZO-2 +
Myc-SIPA1L3 +
FLAG-SJ2BP +
kDa
Input
IP: GFP Trap
IP: SIPA1L3
IP: FLAG Trap
GFP
SIPA1l3
FLAG
C
Input
Capt.
V5-TurboID -dGBP
Cx36-EGFP +Cx36
Strep-HRP
Cx36
EPS15l1
Sec22b
Cx36 transfected
EPS15l1
GPrin1
Overlay
Norm. Intensity
Micron

Figure 6

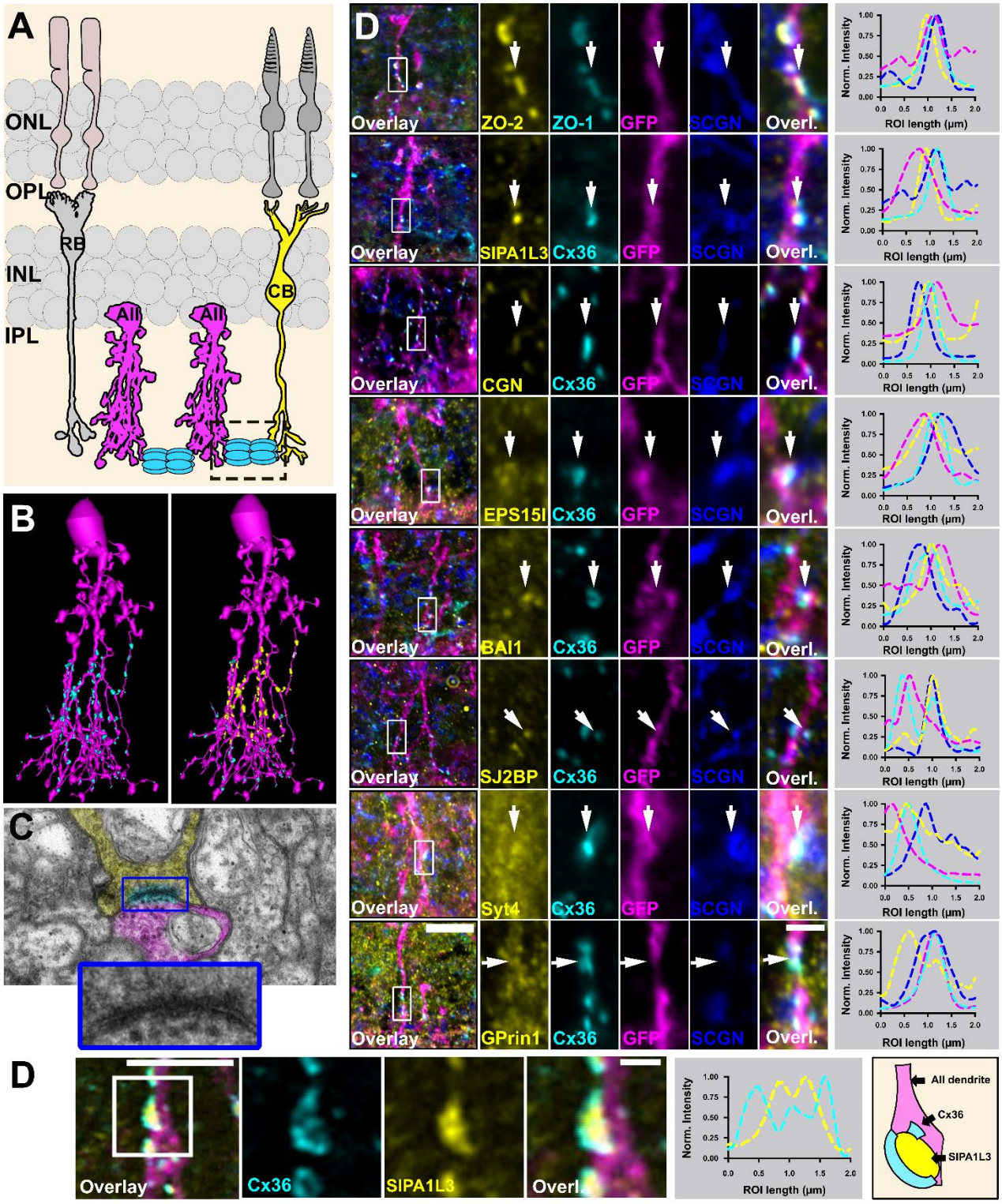
A
ONL
OPL
RB
INL
CB
AII
AII
IPL
B
C
D
Overlay
ZO-2
ZO-1
GFP
SCGN
Overl.
SIPA1L3
Cx36
CGN
EPS15l
BAI1
SJ2BP
Syt4
GPrin1
Norm. Intensity
ROI length (µm)
All dendrite
Cx36
SIPA1L3

Figure 7

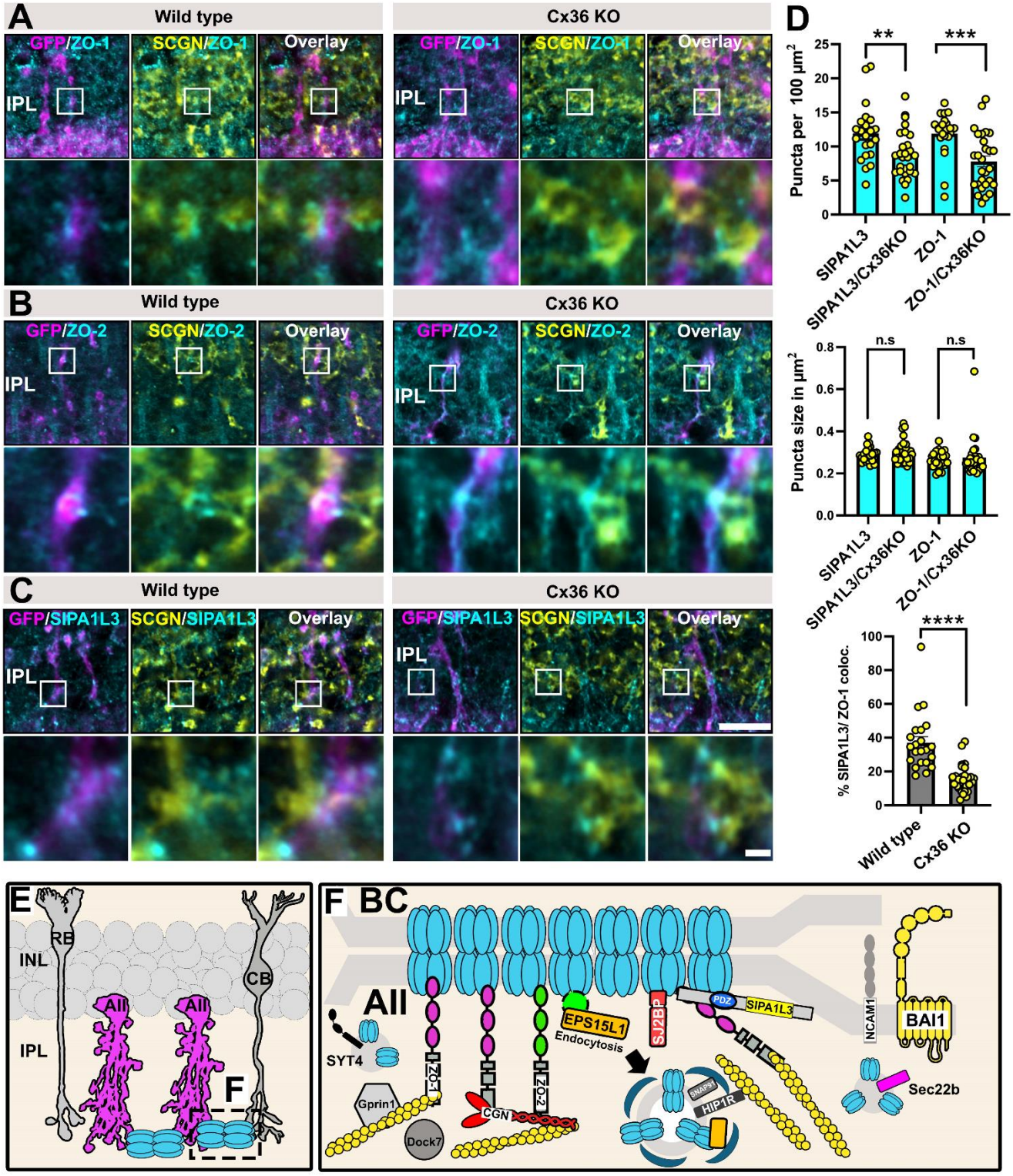
A
Wild type
Cx36 KO
GFP/ZO-1
SCGN/ZO-1
Overlay
IPL
B
GFP/ZO-2
SCGN/ZO-2
C
GFP/SIPA1L3
SCGN/SIPA1L3
D
Puncta per 100 µm²
SIPA1L3
SIPA1L3/Cx36KO
ZO-1
ZO-1/Cx36KO
Puncta size in µm²
n.s
% SIPA1L3/ ZO-1 coloc.
Wild type
Cx36 KO
E
RB
INL
CB
AII
F
BC
SYT4
Gprin1
Dock7
ZO-1
ZO-2
CGN
EPS15L1
Endocytosis
SJ2B2
PDZ
SIPA1L3
SNAP91
HIP1R
NCAM1
BAI1
Sec22b

878 **Supplementary figure 1**

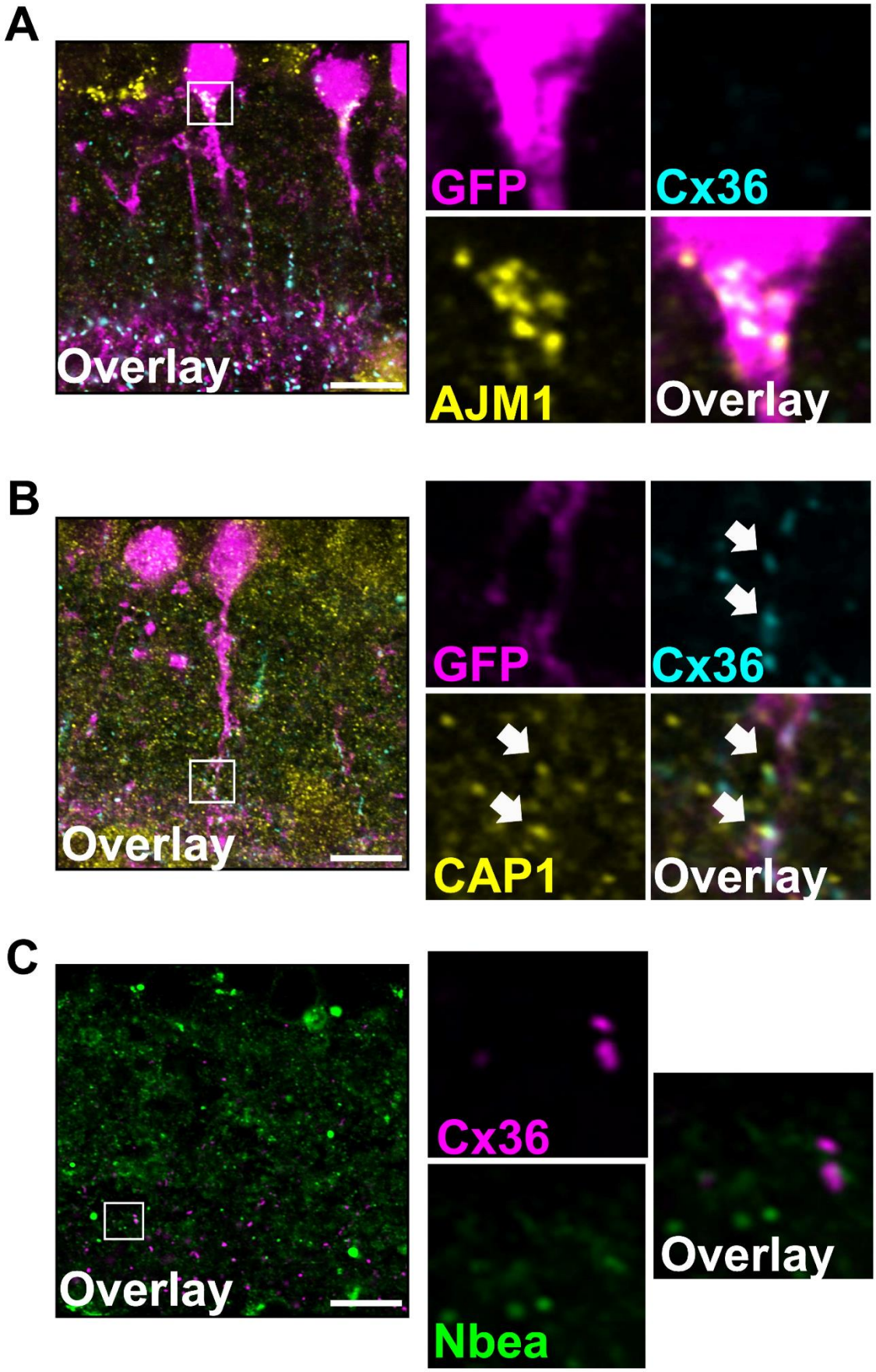

906 **Supplementary figure 2**

907
908
909
910
911
912
913
914
915
916
917
918
919
920
921
922
923
924
925
926
927
928
929
930
931
932
933

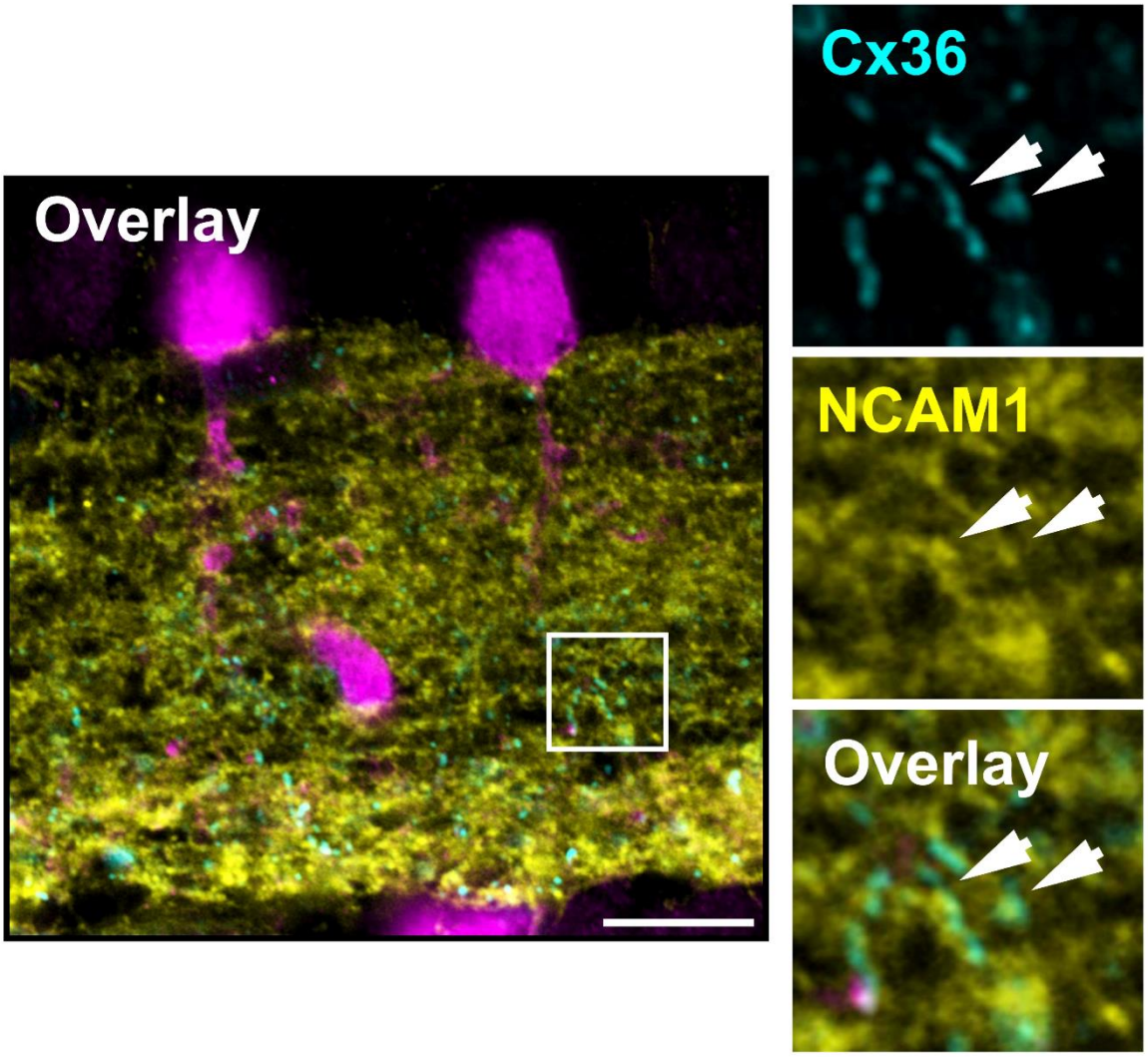

References

1. M. V. Bennett, Electrical synapses, a personal perspective (or history). *Brain research reviews* **32**, 16-28 (2000).
2. C. Sotelo, The history of the synapse. *The Anatomical Record* **303**, 1252-1279 (2020).
3. E. A. Martin, A. M. Lasseigne, A. C. Miller, Understanding the molecular and cell biological mechanisms of electrical synapse formation. *Frontiers in neuroanatomy* **14**, 12 (2020).
4. T. C. Süudhof, Neurotransmitter release. *Pharmacology of Neurotransmitter Release*, 1-21 (2008).
5. M. J. Vaughn, J. S. Haas, On the diverse functions of electrical synapses. *Frontiers in Cellular Neuroscience* **16**, 910015 (2022).
6. S. G. Hormuzdi, M. A. Filippov, G. Mitropoulou, H. Monyer, R. Bruzzone, Electrical synapses: a dynamic signaling system that shapes the activity of neuronal networks. *Biochimica et Biophysica Acta (BBA)-Biomembranes* **1662**, 113-137 (2004).
7. G. Söhl, K. Willecke, Gap junctions and the connexin protein family. *Cardiovascular research* **62**, 228-232 (2004).
8. D. F. Condorelli, N. Belluardo, A. Trovato-Salinaro, G. Mudò, Expression of Cx36 in mammalian neurons. *Brain Research Reviews* **32**, 72-85 (2000).
9. S. A. Bloomfield, B. Völgyi, The diverse functional roles and regulation of neuronal gap junctions in the retina. *Nature Reviews Neuroscience* **10**, 495-506 (2009).
10. V. Serre-Beinier *et al.*, Cx36 makes channels coupling human pancreatic β-cells, and correlates with insulin expression. *Human molecular genetics* **18**, 428-439 (2009).
11. M. Srinivas *et al.*, Functional properties of channels formed by the neuronal gap junction protein connexin36. *Journal of Neuroscience* **19**, 9848-9855 (1999).
12. J. O'brien, The ever-changing electrical synapse. *Current opinion in neurobiology* **29**, 64-72 (2014).
13. W. W. Kothmann *et al.*, Nonsynaptic NMDA receptors mediate activity-dependent plasticity of gap junctional coupling in the AII amacrine cell network. *Journal of Neuroscience* **32**, 6747-6759 (2012).
14. W. W. Kothmann, S. C. Massey, J. O'Brien, Dopamine-stimulated dephosphorylation of connexin 36 mediates AII amacrine cell uncoupling. *Journal of Neuroscience* **29**, 14903-14911 (2009).
15. A. Feigenspan, B. Teubner, K. Willecke, R. Weiler, Expression of neuronal connexin36 in AII amacrine cells of the mammalian retina. *Journal of Neuroscience* **21**, 230-239 (2001).
16. R. E. Marc, J. R. Anderson, B. W. Jones, C. L. Sigulinsky, J. S. Lauritzen, The AII amacrine cell connectome: a dense network hub. *Frontiers in neural circuits* **8**, 104 (2014).
17. C. Del Corsso, R. Iglesias, G. Zoidl, R. Dermietzel, D. C. Spray, Calmodulin dependent protein kinase increases conductance at gap junctions formed by the neuronal gap junction protein connexin36. *Brain research* **1487**, 69-77 (2012).
18. C. Alev *et al.*, The neuronal connexin36 interacts with and is phosphorylated by CaMKII in a way similar to CaMKII interaction with glutamate receptors. *Proceedings of the National Academy of Sciences* **105**, 20964-20969 (2008).
19. J. Lisman, H. Schulman, H. Cline, The molecular basis of CaMKII function in synaptic and behavioural memory. *Nature Reviews Neuroscience* **3**, 175-190 (2002).
20. A. A. Coley, W.-J. Gao, PSD95: A synaptic protein implicated in schizophrenia or autism? *Progress in Neuro-Psychopharmacology and Biological Psychiatry* **82**, 187-194 (2018).
21. S. P. Cárdenas-García, S. Ijaz, A. E. Pereda, The components of an electrical synapse as revealed by expansion microscopy of a single synaptic contact. *Elife* **13**, e91931 (2024).

22. A. C. Miller, A. E. Pereda, The electrical synapse: molecular complexities at the gap and beyond. *Developmental neurobiology* **77**, 562-574 (2017).
23. E. Strettoi, E. Raviola, R. F. Dacheux, Synaptic connections of the narrow-field, bistratified rod amacrine cell (AII) in the rabbit retina. *Journal of Comparative Neurology* **325**, 152-168 (1992).
24. K. J. Roux, D. I. Kim, M. Raida, B. Burke, A promiscuous biotin ligase fusion protein identifies proximal and interacting proteins in mammalian cells. *Journal of cell biology* **196**, 801-810 (2012).
25. T. C. Branon *et al.*, Efficient proximity labeling in living cells and organisms with TurboID. *Nature biotechnology* **36**, 880-887 (2018).
26. T. Takano *et al.*, Chemico-genetic discovery of astrocytic control of inhibition in vivo. *Nature* **588**, 296-302 (2020).
27. M. Artan *et al.*, Interactome analysis of Caenorhabditis elegans synapses by TurboID-based proximity labeling. *Journal of Biological Chemistry* **297** (2021).
28. A. Uezu *et al.*, Identification of an elaborate complex mediating postsynaptic inhibition. *Science* **353**, 1123-1129 (2016).
29. H. Y. Wang, Y.-P. Lin, C. K. Mitchell, S. Ram, J. O'Brien, Two-color fluorescent analysis of connexin 36 turnover: relationship to functional plasticity. *Journal of cell science* **128**, 3888-3897 (2015).
30. H. Li, A. Z. Chuang, J. O'Brien, Photoreceptor coupling is controlled by connexin 35 phosphorylation in zebrafish retina. *Journal of Neuroscience* **29**, 15178-15186 (2009).
31. X. Li, B. Lynn, J. Nagy, The effector and scaffolding proteins AF6 and MUPP1 interact with connexin36 and localize at gap junctions that form electrical synapses in rodent brain. *European Journal of Neuroscience* **35**, 166-181 (2012).
32. S. Tetenborg *et al.*, Phosphorylation of Connexin36 near the C-terminus switches binding affinities for PDZ-domain and 14–3–3 proteins in vitro. *Scientific reports* **10**, 18378 (2020).
33. A. M. Lasseigne *et al.*, Electrical synaptic transmission requires a postsynaptic scaffolding protein. *Elife* **10**, e66898 (2021).
34. C. Ciolofan *et al.*, Association of connexin36 and zonula occludens-1 with zonula occludens-2 and the transcription factor zonula occludens-1-associated nucleic acid-binding protein at neuronal gap junctions in rodent retina. *Neuroscience* **140**, 433-451 (2006).
35. J. O'Brien, H. B. Nguyen, S. L. Mills, Cone photoreceptors in bass retina use two connexins to mediate electrical coupling. *Journal of Neuroscience* **24**, 5632-5642 (2004).
36. Z. Xiong *et al.*, In vivo proteomic mapping through GFP-directed proximity-dependent biotin labelling in zebrafish. *Elife* **10**, e64631 (2021).
37. I. Helbig *et al.*, In vivo evidence for the involvement of the carboxy terminal domain in assembling connexin 36 at the electrical synapse. *Molecular and Cellular Neuroscience* **45**, 47-58 (2010).
38. A. Meyer *et al.*, AII amacrine cells discriminate between heterocellular and homocellular locations when assembling connexin36-containing gap junctions. *Journal of cell science* **127**, 1190-1202 (2014).
39. J. M. Christie *et al.*, Connexin36 mediates spike synchrony in olfactory bulb glomeruli. *Neuron* **46**, 761-772 (2005).
40. H. Khabou *et al.*, Optogenetic targeting of AII amacrine cells restores retinal computations performed by the inner retina. *Molecular Therapy-Methods & Clinical Development* **31** (2023).

41. A. Feigenspan *et al.*, Expression of connexin36 in cone pedicles and OFF-cone bipolar cells of the mouse retina. *Journal of Neuroscience* **24**, 3325-3334 (2004).
42. J. C. Tang *et al.*, Detection and manipulation of live antigen-expressing cells using conditionally stable nanobodies. *Elife* **5**, e15312 (2016).
43. C. E. Flores *et al.*, Trafficking of gap junction channels at a vertebrate electrical synapse in vivo. *Proceedings of the National Academy of Sciences* **109**, E573-E582 (2012).
44. B. Lynn, X. Li, J. Nagy, Under construction: building the macromolecular superstructure and signaling components of an electrical synapse. *The Journal of membrane biology* **245**, 303-317 (2012).
45. C. E. Flores, X. Li, M. V. Bennett, J. I. Nagy, A. E. Pereda, Interaction between connexin35 and zonula occludens-1 and its potential role in the regulation of electrical synapses. *Proceedings of the National Academy of Sciences* **105**, 12545-12550 (2008).
46. S. Tetenborg *et al.*, Trafficking of Connexin36 (Cx36) in the early secretory pathway. *bioRxiv* (2024).
47. E. Leithe, S. Sirnes, T. Fykerud, A. Kjenseth, E. Rivedal, Endocytosis and post-endocytic sorting of connexins. *Biochimica et Biophysica Acta (BBA)-Biomembranes* **1818**, 1870-1879 (2012).
48. E. A. Martin *et al.*, Neurobeachin controls the asymmetric subcellular distribution of electrical synapse proteins. *Current Biology* **33**, 2063-2074. e2064 (2023).
49. Y.-K. Tu, J. G. Duman, K. F. Tolias, The adhesion-GPCR BAI1 promotes excitatory synaptogenesis by coordinating bidirectional trans-synaptic signaling. *Journal of Neuroscience* **38**, 8388-8406 (2018).
50. C. Hartmann *et al.*, The mitochondrial outer membrane protein SYNJ2BP interacts with the cell adhesion molecule TMIGD1 and can recruit it to mitochondria. *BMC Molecular and Cell Biology* **21**, 1-17 (2020).
51. S. Tetenborg *et al.*, Regulation of Cx36 trafficking through the early secretory pathway by COPII cargo receptors and Grasp55. *Cellular and Molecular Life Sciences* **81**, 1-17 (2024).
52. Y. Tsukamoto, N. Omi, Classification of mouse retinal bipolar cells: type-specific connectivity with special reference to rod-driven AII amacrine pathways. *Frontiers in neuroanatomy* **11**, 92 (2017).
53. J. Nagy, B. Lynn, Structural and intermolecular associations between connexin36 and protein components of the adherens junction–neuronal gap junction complex. *Neuroscience* **384**, 241-261 (2018).
54. J. O'Brien, R. Bruzzone, T. W. White, M. R. Al-Ubaidi, H. Ripps, Cloning and expression of two related connexins from the perch retina define a distinct subgroup of the connexin family. *Journal of Neuroscience* **18**, 7625-7637 (1998).
55. A. Dolnik *et al.*, Sipa1l3/SPAR3 is targeted to postsynaptic specializations and interacts with the Fezzin ProSAPiP1/Lzts3. *Journal of Neurochemistry* **136**, 28-35 (2016).
56. R. Greenlees *et al.*, Mutations in SIPA1L3 cause eye defects through disruption of cell polarity and cytoskeleton organization. *Human molecular genetics* **24**, 5789-5804 (2015).
57. J. G. Duman *et al.*, The adhesion-GPCR BAI1 regulates synaptogenesis by controlling the recruitment of the Par3/Tiam1 polarity complex to synaptic sites. *Journal of Neuroscience* **33**, 6964-6978 (2013).
58. M. Westerfield, *The zebrafish book: A guide for the laboratory use of zebrafish Danio (" Brachydanio Rerio")* (University of Oregon, 2007).
59. A. Santhanam *et al.*, A zebrafish model of retinitis pigmentosa shows continuous degeneration and regeneration of rod photoreceptors. *Cells* **9**, 2242 (2020).

60. N. Jin *et al.*, Molecular and functional architecture of the mouse photoreceptor network. *Science advances* **6**, eaba7232 (2020).
61. S. Tetenborg *et al.*, Intralumenal docking of connexin 36 channels in the ER isolates mistrafficked protein. *Journal of Biological Chemistry* **299** (2023).
62. K. Matsuura *et al.*, SIPA1L1/SPAR1 interacts with the neurabin family of proteins and is involved in GPCR signaling. *Journal of Neuroscience* **42**, 2448-2473 (2022).
63. S. Tetenborg, E. Martinez-Soler, O. John, Characterizing ER Retention Defects of PDZ Binding Deficient Cx36 Mutants Using Confocal Microscopy. *Bio-protocol* **14**, e5034 (2024).
64. P. Shannon *et al.*, Cytoscape: a software environment for integrated models of biomolecular interaction networks. *Genome research* **13**, 2498-2504 (2003).
65. G. Bindea *et al.*, ClueGO: a Cytoscape plug-in to decipher functionally grouped gene ontology and pathway annotation networks. *Bioinformatics* **25**, 1091-1093 (2009).
66. D. Szklarczyk *et al.*, The STRING database in 2023: protein–protein association networks and functional enrichment analyses for any sequenced genome of interest. *Nucleic acids research* **51**, D638-D646 (2023).
67. S. Tetenborg *et al.*, Differential distribution of retinal Ca2+/calmodulin-dependent kinase II (CaMKII) isoforms indicates CaMKII-β and-δ as specific elements of electrical synapses made of connexin36 (Cx36). *Frontiers in molecular neuroscience* **10**, 425 (2017).
68. S. Tetenborg *et al.*, Localization of retinal Ca2+/calmodulin-dependent kinase II-β (CaMKII-β) at bipolar cell gap junctions and cross-reactivity of a monoclonal anti-CaMKII-β antibody with Connexin36. *Frontiers in Molecular Neuroscience* **12**, 206 (2019).
69. J. Schindelin *et al.*, Fiji: an open-source platform for biological-image analysis. *Nature methods* **9**, 676-682 (2012).
70. C. L. Sigulinsky, R. L. Pfeiffer, B. W. Jones, Retinal Connectomics: A Review. *Annual Review of Vision Science* **10**, 263-291 (2024).
71. J. R. Anderson *et al.*, A computational framework for ultrastructural mapping of neural circuitry. *PLoS biology* **7**, e1000074 (2009).
72. J. R. Anderson *et al.*, Exploring the retinal connectome. *Molecular vision* **17**, 355 (2011).
73. R. Marc, R. Murry, S. Basinger, Pattern recognition of amino acid signatures in retinal neurons. *Journal of Neuroscience* **15**, 5106-5129 (1995).